



HAL
open science

Physcomitrium patens SMXL homologs are PpMAX2-dependent negative regulators of growth

Ambre Guillory, Mauricio Lopez-Obando, Khalissa Bouchenine, Philippe Le Bris, Alain Lecureuil, Jean-Paul Pillot, Vincent Steinmetz, Francois-Didier Boyer, Catherine Rameau, Alexandre de Saint Germain, et al.

► To cite this version:

Ambre Guillory, Mauricio Lopez-Obando, Khalissa Bouchenine, Philippe Le Bris, Alain Lecureuil, et al.. Physcomitrium patens SMXL homologs are PpMAX2-dependent negative regulators of growth. 2023. hal-04070429

HAL Id: hal-04070429

<https://hal.science/hal-04070429>

Preprint submitted on 15 Apr 2023

HAL is a multi-disciplinary open access archive for the deposit and dissemination of scientific research documents, whether they are published or not. The documents may come from teaching and research institutions in France or abroad, or from public or private research centers.

L'archive ouverte pluridisciplinaire **HAL**, est destinée au dépôt et à la diffusion de documents scientifiques de niveau recherche, publiés ou non, émanant des établissements d'enseignement et de recherche français ou étrangers, des laboratoires publics ou privés.

1 ***Physcomitrium patens* SMXL homologs are PpMAX2-dependent negative** 2 **regulators of growth**

3 Ambre Guillory^{1,2,*}, Mauricio Lopez-Obando^{1,3}, Khalissa Bouchenine¹, Philippe Le Bris¹, Alain
4 Lécureuil¹, Jean-Paul Pillot¹, Vincent Steinmetz⁴, François-Didier Boyer⁴, Catherine Rameau¹,
5 Alexandre de Saint Germain¹, Sandrine Bonhomme^{1,*}

6 ¹Université Paris-Saclay, INRAE, AgroParisTech, Institut Jean-Pierre Bourgin (IJPB), 78000,
7 Versailles, France.

8 ²LIPME, Université de Toulouse, INRAE, CNRS, Castanet-Tolosan 31326, France.

9 ³Institut de biologie moléculaire des plantes (IBMP), CNRS, University of Strasbourg, 12 rue du
10 Général Zimmer, Strasbourg, France.

11 ⁴Université Paris-Saclay, CNRS, Institut de Chimie des Substances Naturelles, UPR 2301, 91198, Gif-
12 sur-Yvette, France.

13 *Corresponding authors: sandrine.bonhomme@inrae.fr and ambre.guillory@inrae.fr

14 **Short title**

15 SMXLs are negative regulators of the MAX2-dependent pathway in *Physcomitrium patens*

16 **Abstract**

17 SMXL proteins are a plant-specific clade of type I HSP100/Clp-ATPases. *SMXL* genes are found in
18 virtually all land plants' genomes. However, they have mainly been studied in angiosperms. In
19 *Arabidopsis thaliana*, three SMXL functional subclades have been identified: SMAX1/SMXL2,
20 SMXL345 and SMXL678. Out of these, two subclades ensure transduction on endogenous hormone
21 signals: SMAX1/SMXL2 are involved in KAI2-ligand (KL) signaling, while SMXL678 are involved in
22 strigolactones (SLs) signaling. Many questions remain regarding the mode of action of these proteins,
23 as well as their ancestral role. In light of recent discoveries in the liverwort *Marchantia polymorpha*, we
24 addressed this second question by investigating the function of the four *SMXL* genes of the moss
25 *Physcomitrium patens*. We demonstrate that PpSMXL proteins are negative regulators of growth,
26 involved in the likely conserved ancestral MAX2-dependent KL signaling pathway. However, PpSMXL
27 proteins expressed in *Arabidopsis thaliana* unexpectedly cannot replace SMAX1/SMXL2 function in
28 KL signaling, whereas they can functionally replace SMXL4/5 and restore root growth. Therefore, the
29 molecular function of SMXL could be conserved, but not their interaction network. Moreover, one
30 PpSMXL clade also positively regulates transduction of the SL signal in *P. patens*, this function most
31 probably having an independent evolutionary origin to angiosperms SMXL678.

32

33 Introduction

34 Strigolactones (SLs) are butenolide compounds with an early origin in land plant evolution (Delaux et
35 al. 2012; Kyojzuka et al. 2022; Bonhomme and Guillory 2022). In angiosperms, these molecules have
36 first been identified as rhizospheric signals with both negative and positive outcomes for the producing
37 plant: SLs stimulate seed germination of root parasitic plants (Cook et al. 1966) but also promote
38 Arbuscular Mycorrhizal (AM) symbiosis (Akiyama et al. 2005) by boosting AM fungi mitochondrial
39 metabolism and thus hyphae growth (Besserer et al. 2006; Besserer et al. 2008). SLs are also employed
40 as phytohormones in angiosperms, where they play diverse roles, in particular regulating plant
41 architecture (for review see (Machin et al. 2020)). Notably, SLs have a largely documented ability to
42 repress axillary branching, by inhibiting axillary bud activity (Gomez-Roldan et al. 2008; Umehara et
43 al. 2008; Jiang et al. 2013; Kerr et al. 2021).

44 Phylogenetic studies suggest that the SL biosynthesis pathway is ancient, genes encoding most SL
45 biosynthesis hormones being found both in land plants and some algae (Delaux et al. 2012; Walker et
46 al. 2019). The CAROTENOID CLEAVAGE DIOXYGENASE 8 (CCD8) enzyme is essential for SL
47 biosynthesis, since its product, carlactone (CL), is considered to be a key precursor for SLs (Alder et al.
48 2012). Genetic studies have demonstrated that CCD8 function, first established in angiosperms models,
49 is probably conserved in bryophytes, as this function was demonstrated at least in the moss
50 *Physcomitrium patens* (*P. patens*) (Proust et al. 2011; Decker et al. 2017) and in the liverwort
51 *Marchantia paleacea* (Radhakrishnan et al. 2020; Kodama et al. 2022). However, this conservation has
52 not been proven yet for algae CCD8 homologs (Walker et al. 2019) and so far, SL synthesis has only
53 been described in land plants. In *P. patens*, SLs have a hormonal function, since PpCCD8-derived
54 compounds repress filament branching and elongation (Proust et al. 2011; Hoffmann et al. 2014), repress
55 gametophore (leafy shoot) basal branching (Coudert et al. 2015) and enhance resistance to
56 phytopathogenic fungi (Decker et al. 2017). Still, the exact molecule with a hormonal role has not been
57 identified yet (Lopez-Obando et al. 2021). In contrast, in *M. paleacea*, the recently characterized SL
58 Bryosymbiol (BSB) does not function as a hormone but is an essential rhizospheric signal needed for
59 AM symbiosis establishment (Kodama et al. 2022).

60 In angiosperms, SL perception is achieved by the receptor DWARF14 (D14). SL perception triggers
61 D14's binding to the F-box protein MORE AXILLARY GROWTH 2 (MAX2), and subsequent
62 targeting of repressor proteins (Bennett et al. 2016). These repressors are encoded by a small gene
63 family, and called SUPPRESSOR OF MAX2 (SMAX)1-LIKE (SMXL) in Arabidopsis (Stanga et al.
64 2013; Soundappan et al. 2015; Wang et al. 2015), and DWARF53 (D53) in rice (Jiang et al. 2013).
65 SMXL6, 7, and 8 are key repressors of the SL pathway for branching control (Soundappan et al. 2015;
66 Wang et al. 2015). SMAX1 and SMXL2 are repressors in a parallel signaling pathway controlling seed
67 germination and seedling development (Stanga et al. 2016). This latter pathway also involves the MAX2

68 F-box protein, and the KARRIKIN INSENSITIVE 2 (KAI2) receptor (Conn and Nelson 2016), an
69 ancestral paralog of D14. While the existence of an endogenous hormonal KAI2-ligand (KL) is expected
70 (Waters et al. 2015; Conn and Nelson 2016; Sun et al. 2016), the identity of molecule(s) activating the
71 so-called KL pathway is still unknown.

72 As described in angiosperms, response to KL or SL requires the degradation of respective SMXL
73 repressors (SMAX1 or SMXL/D53) by the 26S proteasome, via the action of an SCF complex
74 containing MAX2. SMAX1 and SMXL/D53 are large proteins with several conserved structural
75 domains: a double Clp-N domain in N terminus and two ATPase domains (D1 and D2), separated by a
76 middle region (M). The D2 domain is split into D2a and D2b subdomains by an ethylene-responsive
77 element binding factor amphiphilic repression (EAR) motif (for review see (Temmerman et al. 2022)).
78 In the D2a subdomain lies a specific degron motif (RGKT or P loop), necessary for KL/SL-triggered
79 SMXL degradation (Zhou et al. 2013; Khosla et al. 2020). Their activity as repressors partly relies on
80 the EAR motif mediating transcriptional repression (Liang et al. 2016; Ma et al. 2017). Angiosperms
81 possess a third subclade of SMXL proteins, SMXL345, involved in cell differentiation, in a MAX2-
82 independent manner (Wallner et al. 2017; Moturu et al. 2018; Wallner et al. 2020).

83 Members of gene families associated with SL or KL signaling are found in all plants (Walker et al.
84 2019), with the exception of the *D14* SL receptor gene, which likely emerged in the flowering plant
85 lineage. Outside seed plants, putative receptors are homologs to KAI2 (Bythell-Douglas et al. 2017).
86 Thanks to reverse genetics, SL and KL signaling pathways have been partially described in bryophyte
87 models (Proust et al. 2011; Decker et al. 2017; Mizuno et al. 2021; Kodama et al. 2022; Kyojuka et al.
88 2022; Bonhomme and Guillory 2022). In *Marchantia polymorpha*, a KAI2 and MAX2-dependent
89 pathway was recently identified, that regulates thallus growth, and where the unique MpSMXL homolog
90 acts as a repressor (Mizuno et al. 2021). In the moss *P. patens*, we have previously shown that the
91 homolog of MAX2 is not necessary for response to SLs but is involved in the response to red light and
92 possibly in KL signaling (Lopez-Obando et al. 2018; Lopez-Obando et al. 2021). The *KAI2* gene family
93 is extended in *P. patens*, comprising candidate receptors for SLs (GJM clade), and candidate receptors
94 for the KL (euKAI2 clade). Thus, both SL (MAX2-independent) and KL (MAX2-dependent) pathways
95 are present in *P. patens*, in contrast to *M. polymorpha* (Lopez-Obando et al. 2021). Also contrasting
96 with the single SMXL copy of *M. polymorpha*, there are four *PpSMXL* genes. Hence, we have sought
97 to determine whether SMXL proteins' role in the ancestral KL signaling pathway is conserved in *P.*
98 *patens*, and whether the seemingly moss-specific SL signaling pathway also relies on SMXL proteins.

99 Here, we show that the four *PpSMXL* proteins all display the ancestral SMXL domain organization, as
100 well as motifs matching the respective EAR and RGKT consensus (Walker et al. 2019). All four
101 homologs appear to play a negative role downstream of *PpMAX2* in the putative KL signaling pathway
102 of *P. patens*. Introduction of moss *PpSMXL* genes in Arabidopsis failed to induce functional

103 complementation of the *Atsmxl1* mutant, suggesting PpSMXL are not able to form a functional
104 signaling complex with AtKAI2 and AtMAX2. Our results nonetheless support the hypothesis of the
105 ancestral role of SMXL proteins being KL response. Moreover, two PpSMXL proteins could act as
106 positive actors of SL signaling and thus constitute a level of crosstalk between the SL and the PpMAX2-
107 dependent KL pathway. The finding that none of these SMXL homologs are repressors in the SL
108 signaling pathway supports the hypothesis that the mechanism triggering SL signal transduction
109 diverged between *P. patens* and seed plants, even though the same family of receptors was recruited in
110 both lineages (Bythell-Douglas et al. 2017; Lopez-Obando et al. 2021). Furthermore, our work supports
111 the hypothesis that the use of SLs as hormones is not an ancestral land plant trait and might not be shared
112 by seedless plants outside of bryopsid mosses (Kodama et al. 2022).

113

114 **Results**

115 **Phylogeny and expression analysis reveal two clades of SMXL genes in *P. patens***

116 We recovered four SMXL genes from *Physcomitrium patens* (formerly *Physcomitrella patens*)
117 genome on Phytozome (V3.6) as the first four results of a BLAST against *P. patens* proteome, using the
118 full protein sequence of AtSMAX1 (encoded by *AT5G57710.1*). The predicted PpSMXL proteins
119 contain the four regions characteristic of the SMXL family: a double ClpN N-terminal domain (N) and
120 two ATPase domains (D1 and D2) separated by a long middle domain (M) ((Temmerman et al. 2022)
121 and Supplemental Figure S1). As per a previous extensive analysis of SMXL proteins phylogeny
122 (Walker et al. 2019), proteins encoded by *Pp3c2_14220* and *Pp3c1_23530* (here respectively named as
123 *PpSMXLA* and *PpSMXLB*) correspond to a SMXL clade that is specific to bryopsid mosses, while those
124 encoded by *Pp3c9_16100* and *Pp3c15_16120* (*PpSMXLC* and *PpSMXLD* herein) correspond to a
125 SMXL clade that is common to all mosses, including the sphagnopsida (Supplemental Figure S2). At
126 the amino acid level, PpSMXLC and PpSMXLD show 72% identity and PpSMXLA and PpSMXLB
127 61%, whereas comparisons between proteins of the two different clades give 27-29% identity. This
128 suggests these two PpSMXL clades might have been evolving separately since the emergence of the
129 bryopsid lineage.

130 To further explore the putative functional divergence between these two clades, we checked for
131 differences in the expression of the four *PpSMXL* genes. For each *PpSMXL* gene, the region preceding
132 the start codon was cloned upstream of the GUS coding sequence and this construct was introduced into
133 wild-type (WT) moss plants. By staining two-week-old plants from *proPpSMXL:GUS* lines, we found
134 that *PpSMXLA* promoter is hardly active at this age, as staining was only observed at the tip of phyllids
135 (Figure 1A). *PpSMXLC* and *PpSMXLD* promoters seem to be much more active since GUS staining was
136 noted in most of the tissues (Figure 1A). Unfortunately no *proPpSMXLB:GUS* line was obtained. We

137 then investigated these genes' expression along vegetative development, using RT qPCR. With this
138 method, *PpSMXLB* transcripts were detected and we could confirm that gene expression is generally
139 lower in the *PpSMXLA/B* clade than in the *PpSMXLC/D* clade (Figure 1B). Indeed, compared to the
140 mean expression level of *P. patens* genes which is around 16 reads per Kilobase of transcript per million
141 mapped reads (RPKM), *PpSMXLC/D* levels are approximately 18 RPKM and *PpSMXLA/B* levels are
142 around 2 and 6, respectively (Perroud et al. 2018). We could not distinguish any significant changes in
143 transcript levels across *protonema* development, but *PpSMXL* transcript levels all tended to be higher in
144 mature gametophores and/or rhizoids at later developmental stages (Figure 1B).

145

146 ***Ppsmxl* loss-of-function mutants do not display a constitutive SL response phenotype**

147 To investigate the function of the four *PpSMXL* genes in *P. patens* and their potential
148 involvement in the SL/PpKAI2L-GJM or KL/PpMAX2 pathway, we employed two CRISPR-Cas9-
149 based mutagenesis strategies. In the first one, we used only one guide RNA targeted against the CDS
150 region to obtain *Ppsmxl* mutants with frameshift or small insertions/deletions (Lopez-Obando et al.
151 2016b). We ensured obtaining knock-out mutants by devising a second strategy using two guide RNAs,
152 with one targeting each untranslated region (UTR) (Supplemental Figure S1; Supplemental Table S1).
153 Mutations giving rise to a complete deletion of the CDS are noted as *Ppsmxl*Δ (Supplemental Figure S3
154 and S4). Reasoning that the four PpSMXL proteins grouping into two clades could reflect different
155 functions (Supplemental Figure S2 and (Walker et al. 2019)), we first sought double mutants for each
156 clade, e.g. *Ppsmxl*(Δ)*ab* and *Ppsmxl*(Δ)*cd* mutants. Single and double mutants in the *PpSMXLA/B* clade
157 were highly similar to the WT when grown under white light (Figure 2, A and B and Supplemental
158 Figure S5). On the other hand, both *Ppsmxlcd* and *Ppsmxl*Δ*cd* double mutants showed markedly
159 enhanced protonema extension, resulting in very large plants (Figure 2, A and B), even surpassing the
160 *Ppccd8* mutant in some experiments (Supplemental Figure S5). Single *Ppsmxl*Δ*ac* and *Ppsmxld* mutants
161 also tended to be larger than WT, although not to the same level as double mutants (Figure 2, A and B).
162 Thus, it appears *PpSMXLC/D* loss of function results in a protonema extension phenotype opposite to
163 the *Ppmax2-1* mutant, which would be compatible with PpSMXLC/D proteins acting as repressors
164 downstream of PpMAX2.

165 We assayed the phenotypes of the *Ppsmxl* mutants in the dark and continuous red-light, in
166 conditions that allowed us to clearly distinguish mutants affected in the SL pathway from those affected
167 in the PpMAX2-dependent KL pathway (Lopez-Obando et al. 2018; Lopez-Obando et al. 2021).
168 Compared to WT, SL deficient (*Ppccd8*) and SL insensitive (*Ppkai2Lgjm*) mutants elongate more
169 caulonema filaments in the dark. In contrast, KL mutants (*Ppmax2* and *eu-KAI2* clade) elongate fewer
170 filaments than WT in the dark, and develop taller gametophores than WT as a result of an altered
171 photomorphogenesis response to red light (Lopez-Obando et al. 2021).

172 When grown vertically in the dark, *PpSMXLA/B* clade mutants tended to grow as many
173 caulonema filaments as WT, of similar length (Supplemental Figure S6). On the contrary, *PpSMXLC/D*
174 clade mutants developed more and longer caulonema filaments than WT, similarly to *Ppccd8*
175 (Supplemental Figure S6). Additionally, when grown under continuous red light, *PpSMXLA/B* clade
176 mutants showed a similar phenotype to WT, while *PpSMXLC/D* mutants had smaller and more stunted
177 gametophores, again opposite to the *Ppmax2-1* mutant (Figure 2, C to F). Counting phyllid number
178 allowed estimating phytomere length, which was shorter for *PpSMXLC/D* clade mutants than for any
179 other genotype (including *Ppccd8*) (Supplemental Figure S7), suggesting constitutive
180 photomorphogenesis. Overall, *Ppsmxl* mutants' phenotypic characterization suggests that (1) *PpSMXLC*
181 and *PpSMXLD* act redundantly to limit protonema growth, at least partly by limiting caulonema
182 filaments number and length; (2) *PpSMXLC* and *PpSMXLD* activate gametophore photomorphogenesis
183 under red light; (3) *PpSMXLA* and *PpSMXLB* play a very modest role (if any) in regulation of protonema
184 and gametophore growth in various light conditions. Taken together, the results indicate that *Ppsmxlcd*
185 mutants display largely opposite phenotypes to the *Ppmax2-1* mutant, suggesting that *PpSMXLC/D*
186 would act redundantly as repressors of the PpMAX2-dependent KL signaling pathway.

187 Our first mutagenesis strategy also granted us few higher order *Ppsmxl* mutants, of which we
188 characterized one triple mutant (*Ppsmxla1b1d1*) and one quadruple mutant (*Ppsmxla2b2c1d2*). It should
189 be noted that the *Ppsmxlc1* mutation in the quadruple mutant might not cause a loss of function of
190 *PpSMXLC*, as it removed four residues of the protein (not in a predicted functional motif) and did not
191 induce a frameshift (Supplemental Figure S4). Both of these mutants displayed highly restrained growth
192 and browning of the protonema, and only rare stunted gametophores were produced (Supplemental
193 Figure S5A). Moreover, these higher order mutants grew few agravitropic curled caulonema filaments
194 in the dark (Supplemental Figure S6).

195

196 ***PpSMXL* overexpressing lines display phenotypes alike *Ppmax2-1***

197 To further explore the putative role of PpSMXL as repressors of the PpMAX2-dependent
198 pathway, we examined the phenotype of stable *P. patens* transgenic lines overexpressing *PpSMXLA* and
199 *PpSMXLC* with a N-terminal GFP tag under the maize ubiquitin promoter (*pZmUbi:GFP-PpSMXL*
200 lines). We checked the *GFP-PpSMXL* fusion transcript overexpression by semi-quantitative RT-PCR
201 (Supplemental Figure S8A). For clarity, we simplified the notation of these lines as OE-SMXLA and
202 OE-SMXLC, respectively. When grown under standard conditions in white light, these lines were
203 significantly less radially extended than the WT (Figure 3, A and B). OE-SMXLA and OE-SMXLC
204 displayed a growth phenotype similar to that of *Ppmax2-1*, with less (but bigger) gametophores than in
205 WT (Figure 3A and Supplemental Figure S8B). Furthermore, when we examined the phenotype of these
206 lines under red-light continuous illumination, we likewise found that these OE lines behaved very

207 similarly to *Ppmax2-1* (Figure 3, C-D) with very elongated gametophores. Thus, in red light conditions,
208 OE-PpSMXL lines show an opposite phenotype to that of *Ppsmxl* mutants, at least of the *PpSMXLC/D*
209 clade (comparing Figure 2, C-F to Figure 3, C-D). These features point to *PpSMXLC* but also *PpSMXLA*
210 acting downstream of *PpMAX2* and playing an opposite role to *PpMAX2* in development.

211

212 ***PpSMXL* loss-of-function does not restore WT growth in the *Ppccd8* background**

213 To test a putative role of PpSMXL genes in the SL pathway, we combined *Ppccd8* and *Ppsmxl*
214 mutations. Replicating our first CRISPR mutagenesis strategy in the original *Ppccd8* SL deficient
215 background, we obtained *Ppccd8 Ppsmxlab*, *Ppccd8 Ppsmxlcd*, and *Ppccd8 Ppsmxlabcd* mutants.
216 Following the growth of these *Ppccd8 Ppsmxl* mutants (Figure 4; Supplemental Figure S9A), we noticed
217 that mutation of neither SMXL clade restored protonema extension to WT levels. Strikingly, the
218 mutation of all four *PpSMXL* genes, which had a dramatic negative effect on growth in the WT
219 background (Supplemental Figure S5 and S6), was completely circumvented by the *Ppccd8* mutation,
220 and the *Ppccd8 Ppsmxlabcd* quintuple mutant showed a phenotype similar to *Ppccd8*. (Figure 4;
221 Supplemental Figure S9B). It is however worthy of note that the *Ppsmxlc9* mutation in the *Ppccd8*
222 *Ppsmxlabcd* mutant does not lead to a frameshift, similarly to the *Ppsmxlc1* mutation (Supplemental
223 Figure S4), therefore the PpSMXLC protein is likely still functional in this mutant. These observations
224 indicate that PpSMXL proteins are not acting as repressors in the SL pathway. In addition, the lack of
225 functional PpSMXLA, B and D proteins appears to be detrimental only when endogenous SL are
226 present.

227

228 ***PpSMXL* mutations partially restore *Ppmax2-1* mutant phenotypes**

229 To confirm the genetic relationship between *PpSMXL* and *PpMAX2*, we tested whether *Ppsmxl*
230 loss of function could restore a WT phenotype in a *Ppmax2* background. *Ppsmxlab* mutants in the
231 *Ppmax2-1* background were obtained, but no *Ppsmxlcd* mutants. Therefore, we instead mutated
232 *PpMAX2* in one of the *PpsmxlΔcd* mutants, using the CRISPR-Cas9 system, with five guide RNAs
233 targeting *PpMAX2* (Supplemental Figure S10 Supplemental Table S1). Using this approach, we
234 successfully obtained a new *Ppmax2* mutant allele (*Ppmax2-16*) in the *PpsmxlΔcd* mutant background.
235 When we examined the protonema extension of the *Ppmax2 Ppsmxl* mutants, we found that *Ppsmxlab*
236 mutations had no effect on *Ppmax2* mutant phenotype while *Ppsmxlcd* mutations could partially
237 suppress the dramatic growth decrease caused by *PpMAX2* loss of function (Figure 5, A-B). By contrast,
238 under red light, both *Ppsmxlab* and *Ppsmxlcd* mutations could partially restore the excessive elongation
239 of gametophores caused by *PpMAX2* loss of function (Figure 5, C-D).

240 Altogether, phenotype analysis led us to hypothesize that all four PpSMXL proteins could act
241 as repressors of the PpMAX2-dependent KL pathway, with both *PpSMXL* clades acting redundantly in
242 the regulation of gametophore elongation in red light, while *PpSMXLC/D* would play a predominant
243 role under standard light conditions.

244

245 **Loss of PpSMXL C/D function dampens the response to SL mimic but not to KL mimic**

246 We then explored whether *Ppsmxl*(Δ) mutants have a modified phenotypic response to GR24
247 enantiomers. To investigate this response, we relied on the test of filament growth in the dark, which
248 consists in counting the caulonema filaments after enantiomer application (Hoffmann et al. 2014; Lopez-
249 Obando et al. 2021). When treated with 1 μ M (+)-GR24, WT and *Ppccd8* plants developed significantly
250 less caulonema filaments, which is the typical phenotypic response to SL treatment ((Lopez-Obando et
251 al. 2021) and Figure 6A). When investigating the response of *PpsmxlA/B* clade mutants to (+)-GR24, it
252 appeared that all *Ppsmxl* single mutants and *Ppsmxlab* double mutants could respond to this SL mimic,
253 apparently as much as the WT (Figure 6A; Supplemental Figure S11A and S11B). The response of
254 *Ppsmxlcd* double mutants to (+)-GR24 was less pronounced than that of *Ppsmxlab*, considering several
255 independent assays (Figure 6A; Supplemental Figure S11C). *PpSMXLC* and *PpSMXLD* play redundant
256 roles in responding to (+)-GR24, as response was not disturbed in single *Ppsmxlc* and *Ppsmxld* mutants
257 (Supplemental Figure S11B). This suggested that PpSMXLC/D could mediate at least part of the SL
258 response. In addition, single *Ppsmxlc* mutants developed slightly but significantly more filaments than
259 WT in control conditions (Supplemental Figure S11B), possibly indicating that *PpSMXLC* plays a
260 predominant role over *PpSMXLD* in the regulation of filament number.

261 In our previous assays, the use of (-)-GR24 or KAR₂ treatment to trigger the KL pathway gave
262 non-reproducible results, though sometimes tending to increase the filament number (Lopez-Obando et
263 al. 2021). Therefore, we instead chose to evaluate the effect of (-)-desmethyl-GR24, described as a
264 better mimic for KL in both *Arabidopsis* and *Marchantia* (Yao et al. 2021). In similar assays of filament
265 growth in the dark, increasing doses of (-)-desmethyl-GR24 (0.01 to 10 μ M) significantly increased the
266 number of filaments in WT and *Ppccd8* mutant, but not in *Ppmax2-1* mutant (Supplemental Figure S12A
267 and S12B). Unexpectedly, the eu-KAI2 clade mutant, affected in *PpKAI2L-A* to *E* genes encoding
268 putative KL receptors, was responsive to the (-)-desmethyl-GR24 treatment, however not in all assays
269 (Supplemental Figure S12 A and S12B). We still considered (-)-desmethyl-GR24 our best mimic for
270 the KL in *P. patens*. We tested the effect of (-)-desmethyl-GR24 on *Ppsmxl* mutants and observed that
271 both clade A/B and clade C/D *Ppsmxl* double mutants were able to respond to this compound (here
272 tested at 1 and 10 μ M, Figure 6B). However, considering several independent assays with 1 μ M (-)-
273 desmethyl-GR24, the increase of the filament number was lower for the *Ppsmxlcd* double mutant than
274 for the *Ppsmxlab* double mutant (Figure 6B, Supplemental Figure S12C). This observation leads to the

275 hypothesis that all four *PpSMXL* genes may play a redundant role in response to (-)-desmethyl-GR24,
276 at least in this experimental setup (in the dark).

277

278 ***PpSMXL* transcript levels are downregulated in response to activation of the SL signaling pathway**

279 We wondered if a differential transcriptional regulation of all four *PpSMXL* genes could explain
280 the different responses of moss mutants to SL and KL mimics. We therefore compared the transcript
281 levels of *PpSMXL* genes in WT to that in the *Ppccd8* mutant and in the *Ppmax2-1* mutant, and assayed
282 the effect of (+)-GR24 application. Because we previously found that the transcriptional response of
283 SL-related genes was strongly affected by light and enhanced in the dark (Lopez-Obando et al. 2016a;
284 Lopez-Obando et al. 2018), we assessed this response in both dark and light conditions.

285 We observed that all four *PpSMXL* genes have much higher transcript levels in the dark than in
286 the light, in WT, in the *Ppccd8* SL synthesis mutant, and in the *Ppmax2-1* mutant (Supplemental Figure
287 S13, comparing the y-axis in left *versus* right panels). In control conditions, all four *PpSMXL* genes
288 were downregulated in the *Ppmax2-1* mutant compared to WT in the dark (Supplemental Figure S13 A-
289 D, left panels), and also in the light for *PpSMXLC* and *PpSMXLD* (Supplemental Figure S13 A-D, right
290 panels). This suggests that the PpMAX2-dependent KL pathway upregulates the expression of *PpSMXL*
291 genes. In light conditions, *PpSMXLC* and *D* transcript levels in control conditions were higher in *Ppccd8*
292 compared to WT, indicating that endogenous SLs repress the expression of these two genes.
293 Accordingly, the (+)-GR24 treatment down-regulated *PpSMXLC* and *D* transcript levels, in both WT
294 and *Ppccd8* mutant (Supplemental Figure S13, C and D, right panels). Surprisingly, in the *Ppmax2-1*
295 mutant, transcript levels of *PpSMXLC* and *D* were upregulated by the (+)-GR24 treatment in light
296 conditions (Supplemental Figure S13, C and D). Considered together, these results show that *PpSMXL*
297 genes' transcript levels are mainly down-regulated by light and that PpMAX2 function leads to enhanced
298 *PpSMXL* transcription. Hence, expression of *PpSMXL* genes could be induced by activation of the KL
299 pathway. In addition, the down-regulation of *PpSMXLC* and *PpSMXLD* transcripts by SLs further
300 suggests possible crosstalk with the SL pathway.

301

302 **PpSMXL proteins are localized mainly in the nucleus, and not degraded following SL application**

303 Functional nuclear localization signals (NLS) were found in a part of the N-terminal region of
304 AtSMXL7 (Liang et al., 2016) AtSMAX1 (Khosla et al. 2020) and OsSMAX1 proteins (Choi et al.
305 2020). This sequence enriched in residues with basic sidechains is broadly conserved in the four
306 PpSMXL proteins, suggesting they are also located in the nucleus (Supplemental Figure S14).

307 To determine the subcellular localization of PpSMXL proteins, we transiently overexpressed
308 RFP-PpSMXL fusion proteins under the 35S promoter in *Nicotiana benthamiana* epidermal cells stably
309 expressing CFP tagged H2b histone (thus all nuclei were marked by CFP, Supplemental Figure S15). A
310 clear nuclear signal was observed for all four PpSMXL (Supplemental Figure S15A, S15C, S15E,
311 S15G), but some cytoplasmic signal was also observed for RFP fusions with PpSMXLA, PpSMXLB
312 and PpSMXLC. Thus, either the PpSMXL are actually nucleo-cytosolic, or high expression of RFP-
313 PpSMXL under p35S led to proteins in excess leaking out of the nuclear compartment.

314 In angiosperms, the RGKT degron motif is responsible for SMXL proteasomal degradation in
315 presence of SL (Zhou et al. 2013). Since the RGKT motif was found in PpSMXLC and PpSMXLD
316 proteins (RGRT in PpSMXLA and PpSMXLB, Supplemental Figure S1; Supplemental Figure S15I),
317 we obtained constructs where this motif was deleted. In *N. benthamiana* leaves transiently expressing
318 *p35S:RFP-PpSMXL* constructs, we found similarly high levels of RFP-PpSMXL fusion proteins
319 whether the degron motif was present or deleted (Δ RGRT and Δ RGKT lines, Supplemental Figure
320 S15B, S15D, S15F, S15H). Nonetheless, the additional cytosolic RFP signal seemed increased in leaves
321 expressing the Δ RGKT versions of PpSMXL proteins, especially for PpSMXLB and PpSMXLD.

322 Using our stable *P. patens* transgenic lines overexpressing *PpSMXL* (*pZmUbi:GFP-PpSMXL*
323 lines), we could confirm the nuclear localization of PpSMXLA, PpSMXLC and PpSMXLD, even
324 though the GFP signal was not restricted to this compartment for PpSMXLC and PpSMXLD (Figure
325 7). The GFP-PpSMXLB fusion led to a faint and more diffuse cytoplasmic signal. We then tested
326 whether the SL treatment had an effect on GFP-PpSMXL protein stability and/or localization in *P.*
327 *patens*. We could not see any effect of a 20 minute-long 1 μ M (+)-GR24 treatment on the signal observed
328 in the *pZmUbi:GFP-PpSMXLA* line (Supplemental Figure S16A). When introduced into the *Ppmax2-1*
329 mutant background, the GFP-PpSMXLA fusion also led to fluorescent nuclei, that were easier to spot
330 (Supplemental Figure S16B-C). In this background as well, the 1 μ M (+)-GR24 treatment had no effect
331 on the fluorescent signal (Supplemental Figure S16C). These results support the hypothesis that at least
332 PpSMXLA is not a negative regulator of the SL pathway.

333

334 **PpSMXL proteins interact with players of the PpMAX2-dependent pathway**

335 Since we hypothesized the PpSMXL proteins to act in the PpMAX2-dependent KL pathway,
336 we tested putative interactions of these proteins with PpMAX2. Bimolecular fluorescence
337 complementation (BiFC) assays in *P. patens* protoplasts were unsuccessful. However, when
338 overexpressed in *N. benthamiana* cells, each of the four PpSMXL proteins interacted with PpMAX2
339 when respectively fused to complementary parts of the eYFP fluorescent protein (Figure 8, A-D;
340 Supplemental Figure S17). The eYFP signal was lower for PpSMXLA and PpSMXLC, than for
341 PpSMXLB and PpSMXLD, but still indicated a nuclear interaction with PpMAX2 (Figure 8, A, C).

342 Interestingly, we also found that PpSMXLB and PpSMXLD could potentially form homo-oligomers
343 (Figure 8, E, F).

344 Using the same technique, we investigated the interactions of PpSMXL proteins with PpKAI2L proteins,
345 among which the previously reported putative receptors for SL and KL pathways (Lopez-Obando et al.
346 2021). Among the PpKAI2L proteins we tested in BiFC (at least one from each clade), only PpKAI2L-
347 C from eu-KAI2 clade could interact with PpSMXL proteins, moreover the four of them (Figure 8, G-
348 J). This is consistent with our previous demonstration that PpSMXL proteins act in the PpMAX2-
349 dependent pathway since eu-KAI2 genes are also involved in this pathway (Lopez-Obando et al. 2021).
350 To conclude, BiFC assays revealed interactions involving PpSMXL, PpMAX2 and eu-KAI2 putative
351 KL receptors. It is also interesting to note that, while PpSMXL proteins could also be present in the
352 nucleosol in this experimental system, the BiFC signal was strictly restricted to the nuclear compartment.

353 Altogether, our data in *P. patens* allow us to propose a model for PpSMXL role in moss development,
354 highlighting a possible crosstalk between SL and KL-MAX2 pathway (Figure 9 and see discussion).

355

356 **Expression of PpSMXL proteins rescues SMAX4/5 function, but not SMAX1 or SMXL6/7/8** 357 **function in *Arabidopsis***

358 In order to investigate the putative conservation of SMXL proteins function along land plant
359 evolution, we conducted functional complementation assays in *Arabidopsis thaliana*. To this end, one
360 PpSMXL protein from each clade (PpSMXLB and PpSMXLC) was expressed in *Arabidopsis smxl*
361 mutants, under the control of appropriate native promoters from AtSMAX1, AtSMXL5, and AtSMXL6
362 for *Atsmxl1*, *Atsmxl4,5* double and *Atsmxl678* triple mutant complementation, respectively.
363 Furthermore, as positive controls for complementation, the *Arabidopsis SMAX1*, *SMXL5* and *SMXL6*
364 genes, driven by their promoter, were introduced into *Atsmxl* mutants.

365 First, complementation of AtSMXL4/5 function was tested by complementation assays under
366 AtSMXL5 promoter, by measuring the primary root length of young seedlings (Figure 10). We found
367 that all three PpSMXLB and three out of four PpSMXLC expressing lines (Supplemental Figure S18A)
368 had similar root length as WT *Arabidopsis* plants and as the mutant plants complemented with native
369 *AtSMXL5*. This surprising result suggests that both SMXL clades of *P. patens* have retained the same
370 KL and SL-signaling independent function as *Arabidopsis* SMXL homologs.

371 Then, we explored the ability of PpSMXL proteins to functionally replace AtSMAX1, that is to
372 say their capacity to integrate into the KL signaling pathway of *Arabidopsis*. Complementation of
373 AtSMAX1 function was assayed by measuring hypocotyl length of *Atsmxl-2* mutant seedlings
374 expressing PpSMXLB or PpSMXLC (Supplemental Figure S18B) and grown in low light for 11 days
375 (Supplemental Figure S19A). Here we could only achieve partial complementation of *Atsmxl-2*

376 decreased hypocotyl length by reintroducing *pSMAX1:SMAX1*, furthermore only in two out of our three
377 independent transgenic lines (*pSMAX1:SMAX1* #20.6 and #38.1). However, the case of plants
378 expressing *PpSMXLB/C* was still different, as none of the independent lines was even partly restored.
379 Some of them even appeared to develop shorter hypocotyls (*e. g. pSMAX1:PpSMXLB* # 5.4). Thus,
380 although the used *pSMAX1* promoter sequence may not be enough efficient, it seems reasonable to
381 conclude that PpSMXL proteins are not able to replace SMAX1 in Arabidopsis KL signaling.

382 Finally, we explored whether PpSMXL proteins could functionally replace AtSMXL6, by
383 comparing the shoot phenotype of mature transgenic *Atsmxl678* plants expressing PpSMXLB or
384 PpSMXLC (Supplemental Figure S18C) to that of the untransformed *Atsmxl678* mutant (Supplemental
385 Figure S19, B-D). Several shoot phenotypes were assessed, such as plant height, caulinary secondary
386 branch (C2) number, and leaf shape (width). One transformed line out of three independent lines
387 expressing PpSMXLB (#13.2) showed partial complementation of both plant height and C2 number
388 phenotype (Supplemental Figure S19, B-C). However, this line showed no complementation of the leaf
389 width. Leaf width was partially complemented in another transformed line expressing PpSMXLB (#7.7).
390 None of the three independent lines expressing PpSMXLC showed any complementation of shoot
391 phenotype. Hence, it appears PpSMXL proteins are not able to replace SMXL6 in Arabidopsis SL
392 signaling either.

393

394 Discussion

395 SL involvement in mycorrhization and plant architecture implies that these molecules played
396 major roles in land plant evolution, for adaptation to land conditions and then for the emergence of seed
397 plants. The knowledge of SL roles and associated cellular pathways in non-vascular plants is necessary
398 to understand how these compounds could have contributed to the process of terrestrialization.

399 Phylogeny and expression profiles suggest a differential regulation of clade A/B and clade C/D 400 *PpSMXL*

401 It has already been shown that bryopsid mosses have an additional SMXL clade compared to
402 other non-seed plants (Walker et al. 2019). We report evidence of this in *P. patens*, in which
403 *PpSMXLA/B* belong to this divergent clade, which could potentially be neofunctional, as we have shown
404 earlier for some PpKAI2-L homologs (Lopez-Obando et al. 2021). The split between *PpSMXLA* and
405 *PpSMXLB*, and between *PpSMXLC* and *PpSMXLD* on the other hand, is probably quite recent given the
406 high similarity of encoded proteins in each given clade (Supplemental Figure S2). PpSMXLA/B
407 moreover have shorter D1 and M domains compared to PpSMXLC/D (Supplemental Figure S1) and
408 lack the typical degron motif (Supplemental Figure S1 and S15). The consensus RGKT sequence is also
409 modified in some flowering plants SMXL where the motif is nonetheless functional (OsSMAX1 (Zheng

410 et al. 2020)). However, among the sequences examined, PpSMXLA/B are the only one lacking the K
411 residue, which is functionally relevant in Walker A motifs as it is necessary for phosphate binding
412 (Bianchi et al. 2012). Inversely, the EAR motif is conserved in all four PpSMXL proteins, thus
413 transcriptional regulation could be a uniting feature between the two clades.

414 Expression level of *PpSMXLA/B* is lower than that of *PpSMXLC/D* in the protonema (Figure 1).
415 This could indicate that only the C/D clade has a relevant function in the protonema, which is supported
416 by phenotypic analysis of *PpSMXL* mutants. All four *PpSMXL* genes are more highly expressed in older
417 gametophores and/or rhizoids than in filaments, implying that PpSMXL function becomes more
418 important as *P. patens* switches from early vegetative development to mature vegetative development.
419 Furthermore, available RNAseq data (Ortiz-Ramirez et al. 2016), indicate that *PpSMXL* transcripts are
420 even more abundant in spores.

421

422 ***PpSMXL* genes are mainly regulated by light and the PpMAX2-dependent pathway**

423 *PpSMXL* gene expression is mainly downregulated by light, and only modestly sensitive to (+)-
424 GR24 treatments (Supplemental Figure S13). In the light, all four genes tend to be downregulated by
425 (+)-GR24 in WT plants. This trend becomes more evident in the SL deficient *Ppccd8* background, but
426 solely for *PpSMXLC* and *PpSMXLD*, which accordingly have elevated transcript levels in control-
427 treated *Ppccd8* compared to WT. Thus, it appears that only *PpSMXLC* and *PpSMXLD* are significantly
428 repressed by (+)-GR24 and endogenous SLs alike, in the light. The moderate effects of (+)-GR24
429 enantiomer on *PpSMXLC* and *PpSMXLD* expression are of similar amplitude as those reported for
430 angiosperms *SMXL* genes (Stanga et al. 2013; Kerr et al. 2021). However, the feedback regulation
431 exerted by SL on *PpSMXL* transcript levels is opposite to that in angiosperms, since we observed a
432 downregulation of these genes. We relied on the *Ppmax2* mutant as a proxy to explore the effect of the
433 KL pathway on *PpSMXL* gene expression (Supplemental Figure S13). We found that all four *PpSMXL*
434 genes are downregulated in the *Ppmax2* mutant compared to WT in the dark, suggesting that KL
435 signaling would have a positive effect on the transcription of these genes. In the light, only *PpSMXLC*
436 and *PpSMXLD* showed lower transcript levels in the *Ppmax2* mutant compared to WT. This observation
437 is comparable to what was reported for *M. polymorpha*, the unique *MpSMXL* gene being downregulated
438 in *Mpmax2* background (Mizuno et al. 2021). We could hypothesize that PpSMXL proteins bind to the
439 promoters of the *PpSMXL* genes to repress their transcription, as previously described for angiosperm
440 SMXL proteins (Wang et al. 2020). In *Ppmax2*, PpSMXL protein levels are likely very high (from our
441 results, since OE-PpSMXL lines mimic *Ppmax2* phenotype), which would lead to low transcript levels
442 in this mutant. Finally, it was puzzling to observe that (+)-GR24 treatment increased *PpSMXLC* and
443 *PpSMXLD* expression in the *Ppmax2-1* mutant, when the opposite was seen in *Ppccd8*. Thus, SL could

444 somehow prevent the KL-triggered induction of *PpSMXL* transcript levels, perhaps by stabilizing
445 PpSMXL proteins (Figure 9 and see below).

446

447 **PpSMXL proteins take part in nuclear signaling complexes**

448 The presence of predicted NLS sequences, as well as an EAR motif in the four PpSMXL
449 proteins hint at a nuclear localization (Supplemental Figure S1, Supplemental Figure S14). We have
450 shown that all four PpSMXL are indeed located in the nucleus, albeit not exclusively (Figure 7,
451 Supplemental Figures S15). For the moment, we cannot exclude that, as many proteins carrying an NLS,
452 PpSMXL proteins could actually shuttle between nucleus and cytosol, perhaps until a specific signal
453 (KL?) induces their retention into the nuclear compartment. Still, this partial nuclear localization is
454 enough to enable the interaction of PpSMXLs with proteins in the nucleus (namely PpMAX2 and
455 PpKAI2L-C, Figure 8). It would be interesting in the future to explore whether the EAR motif grants
456 PpSMXL proteins a function in transcriptional regulation. Notably, we could determine if they can
457 interact directly with DNA, like has been demonstrated for AtSMXL6 (Wang et al. 2020), and which
458 loci are targeted. In particular, it would be interesting to see whether PpSMXL are able to directly
459 downregulate their own expression, as is the case for AtSMXL6 that binds to the ATAACAA motif in
460 the promoter region of *AtSMXL6* (Wang et al. 2020).

461

462 **PpSMXL proteins are not highly sensitive to SL levels and their sensitivity to KL probably** 463 **depends on light**

464 We report herein that none of the four PpSMXL proteins are rapidly degraded in response to
465 (+)-GR24, not even PpSMXLA, which transcripts are increased by treatment with this enantiomer in
466 the dark (Supplemental Figure S13 and Supplemental Figure S16). Furthermore, when put in the
467 *Ppmax2* background, GFP-PpSMXLA fusion protein was also found insensitive to the (+)-GR24
468 treatment (Supplemental Figure S16C). The absence of (+)-GR24 triggered degradation is probably not
469 the result of an insufficient amount of (+)-GR24 and/or treatment duration, as (1) AtSMXL6 is almost
470 completely degraded after 20 minutes of (\pm)-GR24 2 μ M in p35S:AtSMXL6-GFP seedling (Wang et al.
471 2015); (2) AtSMXL7 is significantly decreased after only 10 minutes of a 1 μ M (\pm)-GR24 treatment in
472 p35S:AtSMXL7-YFP Arabidopsis roots (Soundappan et al. 2015); (3) as little as 12 minutes are
473 necessary for pOsAct:D53-GFP degradation in rice roots (Zhou et al. 2013). Thus, PpSMXL proteins
474 do not behave similarly to AtSMXL6/7 or D53 proteins and they seem insensitive to both the SL mimic
475 (+)-GR24 and endogenous SL from both *P. patens* (GFP lines, Figure 7 and Supplemental Figure S16)
476 and *N. benthamiana* (RFP transient expression lines, Supplemental Figure S15). While their stability in
477 *N. benthamiana* could be explained by an incompatibility with the angiosperm MAX2, PpSMXLs are

478 also stable in *P. patens*. This indicates that PpSMXL proteins are likely not degraded in the context of
479 SL signaling. Likewise, deletion of the degron motif (or degron-like for PpSMXLA/B) has no effect
480 since these proteins are stable (Supplemental Figure S15).

481 The stability of PpSMXLA and PpSMXLC in *P. patens* lines, in the WT background where
482 PpMAX2 is functional, suggests that the whole pool of PpSMXL proteins is not degraded in response
483 to the endogenous compound(s) perceived via PpMAX2 either (putative KL). However, it is important
484 to note that observation of GFP fluorescence was carried out on *P. patens* lines that were previously
485 incubated in low-light conditions or even in the dark for a few hours (Figure 7, Supplemental Figure
486 S16). Since we observed that the intensity of the GFP-PpSMXL signal tended to be lower or even
487 undetectable in high light conditions, it is tempting to hypothesize an activation of the PpMAX2-
488 dependent KL signaling pathway by light, which would lead to PpSMXL degradation. Hence, reported
489 enhanced expression of *PpKAI2-Like* (Lopez-Obando et al. 2016a), *PpMAX2* (Lopez-Obando et al.
490 2018), and *PpSMXL* genes in the dark (Supplemental Figure S13), would be a mean to keep KL signaling
491 active in the absence of light.

492 There might be another link between PpSMXL proteins and SL response. Indeed, we have
493 observed that triple/quadruple *Ppsmxl* mutants display a very striking phenotype seemingly resulting
494 from protonema growth limitation coupled to early senescence. However, this phenotype was fully
495 alleviated by the *Ppccd8* mutation (Figure 4), suggesting that endogenous SLs produced via PpCCD8
496 activity are responsible. We previously showed that SLs have toxic effects at high concentrations on
497 moss growth (Lopez-Obando et al. 2018). Since the *Ppccd8* single mutant does not display this
498 phenotype, we can also infer that PpSMXL proteins would have a protective effect against SL toxicity.

499

500 ***Ppsmxl* loss of function mutants contradict PpSMXL acting as repressors of SL response**

501 At first glance, it is evident that clade C/D *Ppsmxl* mutants do not display a constitutive SL
502 response phenotype, instead they are alike the SL deficient *Ppccd8* mutant (Figure 2; Supplemental
503 Figure S7). This could be indicative of either a positive role of PpSMXLC/D in SL signaling or a
504 negative role of these proteins in PpMAX2-dependent signaling. The phenotype of clade A/B mutants
505 is more comparable to WT, which does not rule out the possibility of PpSMXLA/B acting as repressors
506 of SL signaling (Figure 2). However, both A/B clade and C/D clade loss-of-function in the *Ppccd8*
507 background result in mutants that are like *Ppccd8* (Figure 4; Supplemental Figure S9). If PpSMXL
508 proteins were repressors of SL signaling, the loss of repression should circumvent the absence of
509 endogenous SL and we could expect restoration to a WT-like phenotype. Therefore, PpSMXL are most
510 likely not involved in the repression of the SL response. From our various assays, it appears instead that
511 PpSMXLC and PpSMXLD act redundantly to enable the response to (+)-GR24 in dark-grown
512 caulonema (Figure 6; Supplemental Figure S11), but are not the sole positive regulators of this response.

513 This hypothesis would be in line with the observed repression of *PpSMXLC/D* gene expression by SL
514 (Supplemental Figure S13). Indeed, the SL signal would be transduced through PpSMXLC/D proteins,
515 which would inhibit the expression of their genes, permitting a negative feedback regulation of SL
516 response (Figure 9).

517 *Ppsmxl* and *Ppsmxl*Δ mutations in the same genes have comparable effects on phenotype. Thus,
518 shortened proteins produced from *Ppsmxl* alleles are not functional, even when most of the D1 domain,
519 thought to mediate interaction with receptors (Khosla et al. 2020), is (putatively) still present for the
520 Ppsmx1A, Ppsmx1B and Ppsmx1C mutant proteins (Supplemental Figures S4).

521

522 ***PpSMXL* are negative actors of the PpMAX2-dependent pathway**

523 Two major points of evidence show that PpSMXL proteins are collectively involved in the
524 PpMAX2-dependent signaling pathway and exert a negative role in this pathway: (1) *P. patens* lines
525 overexpressing *PpSMXLA* or *PpSMXLC* are phenotypically similar to the *Ppmax2-1* mutant (Figure 3);
526 (2) Loss of function of either *PpSMXL* clade partially restores developmental disturbances caused by
527 loss of *PpMAX2* function (Figure 5). Although we did not obtain triple or quadruple *Ppsmxl* mutants in
528 the *Ppmax2-1* background, we hypothesize that the four PpSMXL proteins act in an additive fashion to
529 repress PpMAX2-dependent signaling. (3) PpSMXL proteins can indeed interact with components of
530 the PpMAX2-dependent pathway: PpMAX2 itself, but also PpKAI2L-C (Figure 8).

531 We also found that both clades *Ppsmxl* double mutants are able to respond to the KL mimic (–)-
532 desmethyl-GR24, although this response seemed reduced in *Ppsmxlcd* mutants (Figure 6, Supplemental
533 Figure S12C). Thus, the two *PpSMXL* clades likely have a redundant function in the context of
534 PpMAX2-dependent signaling, with PpSMXLC/D playing a prevalent role in the growth conditions we
535 examined. This hypothesis needs to be confirmed by testing the ability of higher order mutants to
536 respond to (–)-desmethyl-GR24, but the dramatic phenotype of these mutants makes them challenging
537 to work with.

538 PpMAX2 is involved in the induction of *PpSMXL* expression, while PpSMXL proteins are
539 likely targets of PpMAX2-dependent degradation. Therefore, PpSMXL could constitute a level of
540 negative feedback regulation in the PpMAX2-dependent pathway. Since this induction by PpMAX2 is
541 especially prevalent in the dark, negative feedback might be more active in the absence of light.
542 Nevertheless, the PpMAX2-dependent regulation of *PpSMXL* expression needs to be further clarified.

543

544 **PpSMXL could be a bridge linking SL signaling and PpMAX2-dependent signaling**

545 It is interesting to note that “de-repression” of PpMAX2-dependent signaling (*Ppsmxlcd*
546 mutants) and “silencing” of SL signaling (*Ppccd8* mutant) have very similar effects on developmental
547 pattern of the protonema (more extended) and gametophores (smaller, especially in red light) (Figure
548 2). This, together with the opposite effects of (+)-GR24 (SL mimic) and (–)-desmethyl-GR24 (KL
549 mimic) on dark-grown caulonema in WT, indicates that these two pathways likely regulate the same
550 processes in opposite manners. In addition, we have previously shown that the *Ppmax2* mutation is
551 epistatic to *Ppccd8* (Lopez-Obando et al. 2018). As suggested in this article, the phenotype of *Ppmax2*
552 would phenocopy a constitutive response to SL, which, according to our present data, would result from
553 an overaccumulation of PpSMXL proteins. This is compatible with a model where SL and KL signaling
554 converge on PpSMXL proteins and regulate their stability/function in opposite manners (Figure 9).

555 One of the processes seemingly regulated by both SL and PpMAX2-dependent pathways, is
556 probably cell division, as demonstrated for the *Ppccd8* mutant (Hoffmann et al., 2014). Increased cell
557 division and filaments branching still must be confirmed in *Ppsmxl* mutants, however, it is supported by
558 the observation that double *Ppsmxl* mutants of both clades (tend to) develop more caulonema filaments
559 than WT in the dark (Figure 6; Supplemental Figure S6). Furthermore, the observation that phenotypic
560 response to (+)-GR24 is not seen in the absence of PpSMXLC/D in some experiments suggests that SL
561 act at least partially via the PpMAX2-PpSMXL pathway. However, as we have seen herein as well as
562 previously (Lopez-Obando et al. 2021), loss of *PpMAX2* function or loss of function in all euKAI2clade
563 does not abolish response to (+)-GR24. Hence, SL signaling does not solely rely on the PpMAX2-
564 dependent pathway, and we can hypothesize that perception of SL by PpKAI2-L proteins of the (GJM)
565 clade does not act via a regulation of the PpMAX2-dependent pathway but nonetheless requires
566 functional PpSMXLC/D. A tempting explanation would be that PpKAI2-L proteins of the GJM clade
567 could interact with and stabilize PpSMXLC/D proteins, thus acting downstream of PpMAX2 and
568 leading to opposite effects on phenotype (Figure 9). While we did not find any direct interaction between
569 PpKAI2-LG/J and PpSMXLC/D using BiFC, the hypothesis that an unknown interactor is needed to
570 permit this interaction is still open.

571

572 **Does PpSMXLC have a specific role among PpSMXL proteins?**

573 We noted that higher-order *Ppsmxl* mutants display highly disturbed growth of gametophores
574 and rapid browning of the protonema, suggesting that extreme activation of the PpMAX2-dependent
575 pathway is very detrimental to viability. The observation that the *Ppccd8* mutation can circumvent the
576 dramatic effect of *Ppsmxlabcd* loss of function (PpSMXLC is probably still functional in the presented
577 mutant) (Figure 4; Supplemental Figure S9), together with our previous hypothesis of SL repressing
578 PpMAX2-dependent signaling, implies that accumulation of PpSMXLC in the absence of other
579 PpSMXL is detrimental to development. Under this hypothesis, in the *Ppccd8* mutant, inhibition of the

580 PpMAX2-pathway by endogenous SL would be lifted and PpSMXLC would be degraded in a
581 PpMAX2-dependent manner.

582

583 **SMXL proteins likely retained a common molecular function along evolution**

584 We have shown through our complementation assays in Arabidopsis that PpSMXLB/C
585 expression in the *Atsmxl45* mutant was enough to restore primary root length to a WT level.
586 Interestingly, it has been reported before that, in Arabidopsis itself, SMXL proteins from different clades
587 can ensure equivalent function if expressed with the same spatio-temporal profile. Indeed,
588 *pAtSMXL5:AtSMAX1* expression in *smxl45* could also complement root growth (Wallner et al. 2017).
589 Hence, all SMXL might have actually kept the same ancestral molecular “growth regulating” function
590 that has been described for SMXL4/5. In angiosperms, this function would have (1) become KL/SL
591 regulated for SMAX1 and SMXL678 clades through the evolutive gain of interaction with KAI2/KAI2L
592 receptors and with MAX2, (2) become differentially regulated in various types of tissues and
593 developmental contexts through major changes in regulatory sequences.

594 On the other hand, the observation that PpSMXL expression does not complement the *Atsmxl1*
595 mutant is not surprising, given that our previous attempt to complement the *Atmax2* mutant with
596 PpMAX2 was also unsuccessful (Lopez-Obando et al. 2018). Hence, we could think that, despite MAX2
597 and SMAX1/PpSMXL acting in a conserved KL signaling pathway in both species, the interface for
598 MAX2/SMXL interaction is simply not compatible between Arabidopsis and *P. patens* proteins. The
599 same could be concluded from the absence of complementation in the *smxl678* mutant.

600 The MpKAI2a/MpMAX2 pathway, regulating thallus and gemmae growth in *M. polymorpha*
601 through the degradation of the unique MpSMXL repressor (Mizuno et al. 2021) is so far the “simplest”
602 form described of the above-described ancestral growth regulating function. It is interesting to note that
603 in *M. polymorpha*, like in *P. patens*, this pathway is regulated by light. *M. polymorpha* does not
604 synthesize SLs (no CCD8), and therefore the crosstalk between SL and KL pathways that we highlight
605 in *P. patens* cannot be observed. This crosstalk is also apparently absent in *M. paleacea* though it
606 synthesizes BSB, likely because of the absence of the required receptor for SL as hormones (Kodama
607 et al. 2022). Therefore, *P. patens* would represent a specific case among bryophytes where the SL and
608 KL pathway are interconnected. The identity of both SL and KL signals remains to be discovered.

609

610 **Methods**

611 **Cultivation of *Physcomitrium patens* Gransden**

612 Unless otherwise explicitly stated in legends, experiments were always carried out on PpNO₃ medium
613 (corresponds to the minimal medium described by Ashton et al., 1979), in the following control
614 conditions: 25°C during daytime and 23°C at night, 50% humidity, long days conditions with 16 hours
615 of day and 8 hours of night (quantum irradiance of ~80 μmol/m²/s). Multiplication of tissues from young
616 *protonema* fragments prior to every experiment is done in the same conditions but using medium with
617 higher nitrogen content (PpNH₄ medium, PpNO₃ medium supplemented with 2.7 mM NH₄ tartrate). For
618 red light experiments, plants were grown on PpNO₃ medium in Magenta pots at 25°C, in continuous
619 red-light (~45 μmol μmol/m²/s). Cellophanes of appropriate sizes were used for monitoring of
620 *protonema* extension kinetics, as well as for the cultures launched in 6-well plates for gene expression
621 studies (see a detailed protocol in our methods chapter titled “Methods for medium-scale study of the
622 biological effects of strigolactone-like molecules on the moss *Physcomitrella patens*”). Analysis of
623 caulonema growth in the dark was performed in 24-well plates, with ~2 weeks of growth in control
624 conditions before incubation (± treatment) in the dark and placed vertically for ~10 days (see the same
625 method chapter).

626 ***P. patens* gene expression analyses by qPCR**

627 Total *P. patens* RNA was extracted and rid of contaminant genomic DNA using RNeasy Plant Mini Kit
628 and on-column DNase I treatment (Qiagen), following supplier’s indications. cDNA was obtained using
629 the MaximaTM H Minus retrotranscriptase (ThermoFisher), from 50-250 ng of total RNA. cDNA extracts
630 were diluted at 1/5-1/8 before use. RT qPCR was performed in a 384-well thermocycler
631 (QuantStudioTM5, ThermoFisher), using SsoAdvanced Universal SYBR Green Supermix (BioRad) and
632 appropriate primers. The thermocycler was programmed to run for 3 min at 95°C, followed by 40-45
633 cycles of 10 sec at 95°C and 30 sec at 60°C. Each biological replicate was run twice to assess technical
634 variation. Expression of genes of interest was normalized by two reference genes among *PpElig2*
635 (*Pp3c14_21480*), *PpAPT* (*Pp3c8_16590*) and *PpACT3* (*Pp3c10_17080*) (all three are expressed at
636 similar levels (Le Bail et al. 2013). Relative expression was calculated as $RE = 2^{-CT_{\text{gene}}/2 - CT_{\text{ref}}}$ where
637 CT_{ref} is the mean value of the two reference genes. For the study of *PpSMXL* genes’ expression across
638 development (figure 2), WT *P. patens* was cultivated in petri dishes from fragmented tissues, or in
639 Magenta pots (for 35 days). The following tissues were collected: protonema at 6 days (mostly
640 chloronema in our culture conditions), at 10 days (mix of chloronema and caulonema), and at 14 days
641 (mix of chloronema, caulonema and buds), and mature gametophores and rhizoids at 35 days. Four
642 biological replicates were used for each timepoint. For the “response to GR24” experiment, plants were
643 cultivated from fragmented *protonema* in 6-well plates for 2 weeks in control conditions, then
644 transferred in the dark for one week, and treated with 1 μM (+)-GR24, or 0.01% DMSO in the dark for
645 6 hours. Six biological repeats were used for each genotype and treatment. For the “response to light”
646 experiment, 2-week-old WT, *Ppccd8* and *Ppmax2-1* were similarly transferred in the dark for 5 days,
647 and then either kept in the dark for 24 hours, kept in control white light conditions for 24 hours, or placed

648 under constant red-light for 1, 6 or 24 hours. Six biological repeats were used for each genotype and
649 treatment.

650 **Cloning of *PpSMXL* CDS and promoters**

651 Coding sequence of each *PpSMXL* gene was amplified on WT *P. patens* Gransden cDNA, using Phusion
652 DNA polymerase (ThermoFisher), following provided instructions and using primers with attB1 and
653 attB2 extensions (respectively on the forward and reverse primer, see Supplemental Table 1). A similar
654 strategy was used to amplify promoter sequences (full 5'UTR and 1000 bp upstream, from Phytozome
655 V3.1). Both CDS and promoters were then integrated into the pDONR207 plasmid using BP clonase II
656 mix (Thermofisher). pDONR207 plasmids containing *PpSMXL* CDS were submitted to PCR-mediated
657 mutagenesis to obtain Δ RGK/RT versions.

658 **CRISPR-Cas9 mediated mutagenesis**

659 Coding sequences of *PpSMXL* and *PpMAX2* were used to search for CRISPR RNA (crRNA) contiguous
660 to a PAM motif recognized by *Streptococcus pyogenes* Cas9 (NGG), using the webtool CRISPOR V4
661 against *P. patens* genome Phytozome V9 (<http://crispor.tefor.net/>). crRNAs located in the first third of
662 the coding sequence, with highest possible specificity score, and fewest possible predicted off-targets,
663 were selected. Small constructs containing each crRNA fused to either the proU6 or the proU3 snRNA
664 promoter in 5' U3 or U6 promoter (Collonnier et al. 2017), and to the tracrRNA in 3', encased between
665 attB1/attB2 Gateway recombination sequences, were synthesized by Twist Biosciences. These inserts
666 were then cloned into pDONR207 vectors. Polyethylene glycol-mediated protoplast transformation was
667 performed with multiple pDONR207-sgRNA according to the protocol described by Lopez-Obando et
668 al., 2016. Mutations of the *PpSMXL* genes were confirmed by PCR amplification of *PpSMXL* loci
669 around the recognition sequence of each guide RNA and sequencing of the PCR products. Alternatively,
670 for *PpSMXL* genes, a second strategy was employed where crRNAs were designed in the 5' and 3'UTR
671 sequences, to completely remove the coding sequence of *PpSMXL* genes from the genome when used
672 together. Mutants obtained from this second strategy were genotyped by monitoring the size and
673 sequence of amplicons spanning from the 5'UTR to the 3'UTR.

674 **Generation of *proPpSMXL:GUS*, *proZmUbi:GFP-PpSMXL* and control *proZmUbi:flag-GFP* lines**

675 *proPpSMXL:GUS* constructs were obtained by LR recombination of pDONR207 plasmids containing
676 *PpSMXL* promoters with the pMP1301 destination vector previously described (Lopez-Obando et al.,
677 2018). This method could not be employed for the promoter of *PpSMXLA*, which had to be amplified
678 with a NotI forward primer and a AscI reverse primer and was subcloned into the pTOPO-blunt II vector
679 (ThermoFisher), and then directly inserted into a NotI-AscI digested pMP1301. *proZmUbi:GFP-*
680 *PpSMXL* constructs were obtained by LR recombination of pDONR207 plasmids containing *PpSMXL*
681 coding sequences with the pMP1335 destination vector

682 (http://labs.biology.ucsd.edu/estelle/Moss_files/pK108N+Ubi-mGFP6-GW.gb). Similarly, the
683 *proZmUbi:flag-GFP* construct was obtained using the pMP1382 destination vector. These plasmids
684 were used independently to transform WT *P. patens* Gransden, together with pDONR207 containing
685 sgRNA recognizing Pp108 homology sequences contained in the three pMP vectors and appropriate
686 Cas9 and selection plasmids (Lopez-Obando et al., 2016b). Obtained G418 resistant lines were screened
687 for insertion using PCR (with proPpSMXL forward and GUS reverse, GFP forward and PpSMXL
688 reverse, or proZmUbi forward and GFP reverse primers, respectively).

689 **GUS staining**

690 Two to six independent G418 resistant lines with verified *GUS* insertion into the genome were obtained
691 for each *PpSMXL* genes except *PpSMXLB* and used for histochemical analyses. GUS staining of two-
692 week-old *P. patens* plants was carried out following the protocol detailed by Yuji Hiwatashi on the
693 NIBB PHYSCObase website (<http://moss.nibb.ac.jp/protocol.html>).

694 **Generation of BiFC constructs**

695 Gateway cloned inserts of genes of interest were integrated into pbiFP vectors using LR Clonase II mix
696 (ThermoFisher). Inserts containing a STOP codon were cloned in pbiFP2 and pbiFP3, those not
697 containing a STOP were cloned in pbiFP1 and pbiFP4 (when possible, all four vectors were obtained
698 for a given gene). Resulting vectors were electroporated into *Escherichia coli* DH10B cells and clones
699 were selected on spectinomycin. In phase integration of the coding sequence relative to the half eYFP
700 tag was checked by sequencing insert's ends. The previously published GLOBOSA/DEFICIENS
701 interaction (Azimzadeh et al. 2008) was consistently used a positive control of eYFP reconstruction.

702 **Agroinfiltration of *Nicotiana benthamiana* leaves**

703 pbiFP plasmids containing the genes of interest were electroporated into *Agrobacterium tumefaciens*
704 strain C58C1. Agrobacteria were incubated for 18 hours at 28°C under constant agitation and then
705 pelleted, washed twice, and resuspended in infiltration buffer (13 g/L S-medium (Duchefa Biochemie)
706 and 40 g/L sucrose, pH 5.7 with KOH) to attain an OD600 value of 0.5. To enhance transient expression
707 of RFP-PpSMXL and BiFC fusion proteins, the P19 viral suppressor of gene silencing from tomato
708 bushy stunt virus was co-expressed. Equal volumes of needed bacterial cultures were mixed and
709 infiltrated into the abaxial epidermis of 4–5-week-old *Nicotiana benthamiana* leaves. After incubation
710 at 25 °C (16 h light/8 h dark) for 4 days, leaves were harvested on wet paper and kept in similar
711 temperature and hygrometry conditions for short-term preservation until observation.

712 **Confocal microscopy observations**

713 Fragments of *P. patens proZmUBI:GFP-PpSMXL* plants and infiltrated parts of *Nicotiana benthamiana*
714 leaves were both observed on a TCS SP5 inverted or on a TCS SP8 Upright confocal microscopy system

715 (Leica), with a 20X objective. GFP fluorescence was acquired in the 495nm-520nm λ range, eYFP in
716 the 525nm-540nm range, RFP in the 570nm-610nm range and CFP in the 465nm-505nm range. Signals
717 in the 700nm-750nm range were attributed to chlorophyll autofluorescence. Lasers used for excitation
718 have a peak wavelength of 488nm (GFP), 514nm (YFP), 458nm (CFP) and 561nm (RFP).

719 **Constructs and generation of Arabidopsis transgenic lines**

720 The expression vectors for transgenic Arabidopsis were constructed by MultiSite Gateway Three-
721 Fragment Vector Construction kit (Invitrogen). AtSMAX/SMXL and PpSMXL constructs were tagged
722 with m-Citrine protein at their C-terminus. Lines were resistant to hygromycin. For the Arabidopsis
723 *SMAX1* (AT5G57710), *SMXL5* (A5G57130) and *SMXL6* (AT1G07200) promoters cloning, a 3128-bp
724 fragment upstream from SMAX1 start codon, a 3028-bp fragment upstream from SMXL5 start codon
725 and a 3058-bp fragment upstream from SMXL6 start codon were amplified from Col-0 genomic DNA
726 using the primers described in Supplemental Table S1, and were cloned into the pDONR-P4P1R vector,
727 using Gateway recombination (Invitrogen) as described in (Lopez-Obando et al. 2021). The m-Citrine
728 tag was cloned into pDONR-P2RP3 (Invitrogen) as described in (de Saint Germain et al. 2016).
729 AtSMAX1, AtSMXL5 and AtSMXL6 CDS were PCR amplified from Arabidopsis Col-0 cDNA and
730 with the primers specified in Supplemental Table S1 and then recombined into the pDONR221 vector
731 (Invitrogen). PpSMXLB and PpSMXLC CDS were obtained as described above. The suitable
732 combinations of AtSMXL native promoters, AtSMXL or PpSMXL CDS, and m-Citrine tag were cloned
733 into the pH7m34GW final destination vectors by using the three fragment recombination system (Karimi
734 et al. 2007) and were thusly named *pSMAX1:SMAX1*, *pSMAX1:PpSMXLB*, *pSMAX1:PpSMXLC*,
735 *pSMXL5:SMXL5*, *pSMXL5:PpSMXLB*, *pSMXL5:PpSMXLC*, *pSMXL6:SMXL6*, *pSMXL6:PpSMXLB*
736 and *pSMXL6:PpSMXLC*. Transformation of Arabidopsis *smx1-1*, *smx4-1* *smx5-1* and *smx6/7/8*
737 mutants was performed according to the conventional floral dipping method (Clough and Bent 1998),
738 with Agrobacterium strain GV3101. For each construct, at least 12 independent T1 lines were isolated,
739 and then 2 to 4 lines were selected in T2 for showing a 3 :1 segregation (single T-DNA insertion).
740 Phenotypic analysis shown in Figure 10 and Supplemental Figures S18 and S19 were performed on the
741 T3 homozygous lines.

742 **Plant materials, growth conditions, and phenotypic assays**

743 *Arabidopsis thaliana* plants used in this study originated from the Columbia (Col-0) ecotype
744 background. *smx1-2* and *smx6/7/8* Arabidopsis mutants are gift Dave Nelson (University of California,
745 Riverside), and the Arabidopsis *smx4-5* mutant gift from Thomas Greb (Heidelberg University,
746 Heidelberg). The transgenic lines are described above. For *Arabidopsis thaliana* shoot branching assays,
747 the plants were grown in greenhouse. Experiments were carried out in summer, under long photoperiods
748 (15-16 h per day); daily temperatures fluctuated between 18 °C and 25 °C. Peak levels of PAR were
749 between 700 and 1000 $\mu\text{mol m}^{-2} \text{s}^{-1}$. Plants were watered twice a week with tap water. The number of

750 caulinary branch and plant height was scored when the plants were 35 days old. Leaf Morphology Assay
751 was performed as described in (Soundappan et al. 2015) on the 5th leaf of each plant marked with
752 indelible marker at 3 weeks post-germination. Plants were cultivated as for branching assay. 12 plants
753 were then used for Kruskal Wallis Dunn *post-hoc* test VS Col0. Hypocotyl elongation assays were
754 performed as described in (Guercio et al. 2022) with the following modification: 11-day-old seedlings
755 were photographed and hypocotyl lengths were quantified using ImageJ. 2 plates of 20 to 24 seeds were
756 sown for each genotype. The data from the 45 seedlings were then used for a one-way ANOVA de
757 Welch, Dunnett T3 *posthoc* VS Col0 (n = 45-129, p<5%). For lateral Root Assay seedlings were grown
758 on 3 different plates in the same media and condition as for hypocotyl assay. Roots were analyzed at 15
759 days post-germination (dpg). Primary root length was then measured using ImageJ. 24 seedlings per
760 genotype were used for Kruskal Wallis followed by a Dunn *post-hoc* test.

761

762 **Chemicals**

763 GR24 enantiomers and (-)-desmethyl-GR24 were produced by V Steinmetz and F-D Boyer using
764 organic synthesis and chiral separation as described in (de Saint Germain et al. 2021). Chemicals were
765 diluted in DMSO.

766

767 **RT-PCR analysis in Arabidopsis**

768 Semi-quantitative RT-PCR analyses of Arabidopsis transformants were performed from leaf or seedling
769 RNAs extracted and rid of contaminant genomic DNA using RNeasy Plant Mini Kit and on-column
770 DNase I treatment (Qiagen), following supplier's indications. cDNA was obtained using the H Minus
771 retrotranscriptase (ThermoFisher), from 250 ng of total RNA. cDNA extracts were diluted twice, and
772 1µL was used for each PCR reaction. The thermocycler was programmed to run for 3 min at 95 °C,
773 followed by 28 cycles of 30 sec at 95 °C, 30 sec at 56 °C and 40 sec at 72 °C.

774 **Statistical analysis of results**

775 Kruskal-Wallis, Mann-Whitney and *post-hoc* Dunn, Dunnett or Tukey multiple comparisons tests
776 (details in figures legends) were carried out either in R 3.6.3 or in GraphPad Prism 8.4.2. Tests employed
777 were mostly non-parametric as normality of distributions and/or homoscedasticity among groups could
778 not be confirmed in most experiments (Kruskal-Wallis tests for multiple comparisons and Mann-
779 Whitney for single comparisons, unless otherwise stated in legends). For some gene expression
780 experiments, data points were excluded based on an outliers' search (Grubb's, $\alpha=0.05$) on in GraphPad
781 Prism 8.4.2. Unless otherwise defined, used statistical significance scores are as follow: # $0.05 \leq p < 0.1$,
782 * $0.01 \leq p < 0.05$, ** $0.001 \leq p < 0.01$, *** $p < 0.001$. Same letters scores indicate that $p \geq 0.05$ (non-significant
783 differences).

784 **Accession Numbers**

785 Moss sequences used in the present article can be found on Phytozome (*P. patens* Gransden genome,
786 V3.1 version). *PpSMXLA* is *Pp3c2_14220*, *PpSMXLB* is *Pp3c1_23530*, *PpSMXLC* is *Pp3c9_16100* and
787 *PpSMXLD* is *Pp3c15_16120*. *PpMAX2* corresponds to *Pp3c17_1180*, *PpCCD8* to *Pp3c6_21520*,
788 *PpAPT* to *Pp3c8_16590*, *PpACT3* to *Pp3c10_17080*, and *PpElig2* corresponds to *Pp3c14_21480*.

789 **Authors contributions**

790 A.G and S.B are the main authors of the manuscript and A.G performed most of the experiments.
791 Some steps in genotyping mutant and transgenic lines and support with molecular cloning was given by
792 P.L.B, K.B, A.L and S.B helped for moss mutant phenotyping and J-P. P for transgenic Arabidopsis
793 phenotyping. V.S and F-D. B furnished SL and KL analogs. Plasmids used for *Ppsmxl* mutant generation
794 in the first strategy, as well as higher order *Ppsmxl* mutants were obtained by M.L-O. A.G, S.B, A.S.G,
795 and C.R all contributed to experimental design and to the argumentation developed herein.

796

797 **Acknowledgements**

798 We thank Dave Nelson (University of California, Riverside) for the generous gift of Arabidopsis
799 *smxl-2* and *smxl678* mutants, as well as for the SMXL6p:SMXL6-GFP construct. We thank Thomas
800 Greb (Heidelberg University, Heidelberg) for the kind gift of Arabidopsis *smxl4-5* mutant. We thank
801 Fabien Nogu  (IJPB, Versailles) for his helpful advice and for giving us guide RNAs targeting the Pp108
802 non-coding locus. We thank Martine Pastuglia (IJPB, Versailles) for the gift of BiFC control constructs
803 and Michael J. Prigge (University of California San Diego, La Jolla) for nicely sending us the pMP
804 destination vectors. This work has benefited from the support of IJPB's Plant Observatory technological
805 platforms.

806

807 **Fundings**

808 The IJPB benefits from the support of Saclay Plant Sciences-SPS (ANR-17-EUR-0007). This work
809 has benefited from a French State grant (Saclay Plant Sciences, reference n  ANR-17-EUR-0007,
810 EUR SPS-GSR) managed by the French National Research Agency under an Investments for the
811 Future program integrated into France 2030 (reference n  ANR-11-IDEX-0003-02).

812

813 **References**

814 Akiyama K, Matsuzaki K, Hayashi H (2005) Plant sesquiterpenes induce hyphal branching in arbuscular
815 mycorrhizal fungi. *Nature* 435 (7043):824-827. doi:10.1038/nature03608

- 816 Alder A, Jamil M, Marzorati M, Bruno M, Vermathen M, Bigler P, Ghisla S, Bouwmeester H, Beyer P,
817 Al-Babili S (2012) The path from beta-carotene to carlactone, a strigolactone-like plant
818 hormone. *Science* 335 (6074):1348-1351. doi:10.1126/science.1218094
- 819 Azimzadeh J, Nacry P, Christodoulidou A, Drevensek S, Camilleri C, Amiour N, Parcy F, Pastuglia M,
820 Bouchez D (2008) Arabidopsis TONNEAU1 proteins are essential for preprophase band
821 formation and interact with centrin. *Plant Cell* 20 (8):2146-2159. doi:tpc.107.056812 [pii]
822 10.1105/tpc.107.056812
- 823 Bennett T, Liang Y, Seale M, Ward S, Muller D, Leyser O (2016) Strigolactone regulates shoot
824 development through a core signalling pathway. *Biol Open* 5 (12):1806-1820.
825 doi:10.1242/bio.021402
- 826 Besserer A, Becard G, Jauneau A, Roux C, Sejalon-Delmas N (2008) GR24, a synthetic analog of
827 strigolactones, stimulates the mitosis and growth of the arbuscular mycorrhizal fungus
828 *Gigaspora rosea* by boosting its energy metabolism. *Plant Physiol* 148 (1):402-413
- 829 Besserer A, Puech-Pages V, Kiefer P, Gomez-Roldan V, Jauneau A, Roy S, Portais JC, Roux C, Becard
830 G, Sejalon-Delmas N (2006) Strigolactones stimulate arbuscular mycorrhizal fungi by
831 activating mitochondria. *PLoS Biol* 4 (7):e226
- 832 Bianchi A, Giorgi C, Ruzza P, Toniolo C, Milner-White EJ (2012) A synthetic hexapeptide designed to
833 resemble a proteinaceous P-loop nest is shown to bind inorganic phosphate. *Proteins* 80
834 (5):1418-1424. doi:10.1002/prot.24038
- 835 Bonhomme S, Guillory A (2022) Synthesis and Signalling of Strigolactone and KAI2-Ligand signals in
836 bryophytes. *J Exp Bot*. doi:10.1093/jxb/erac186
- 837 Bythell-Douglas R, Rothfels CJ, Stevenson DWD, Graham SW, Wong GK, Nelson DC, Bennett T
838 (2017) Evolution of strigolactone receptors by gradual neo-functionalization of KAI2
839 paralogues. *BMC biology* 15 (1):52. doi:10.1186/s12915-017-0397-z
- 840 Choi J, Lee T, Cho J, Servante EK, Pucker B, Summers W, Bowden S, Rahimi M, An K, An G,
841 Bouwmeester HJ, Wallington EJ, Oldroyd G, Paszkowski U (2020) The negative regulator
842 SMAX1 controls mycorrhizal symbiosis and strigolactone biosynthesis in rice. *Nat Commun*
843 11 (1):2114. doi:10.1038/s41467-020-16021-1
- 844 Clough SJ, Bent AF (1998) Floral dip: a simplified method for *Agrobacterium*-mediated transformation
845 of *Arabidopsis thaliana*. *Plant J* 16 (6):735-743. doi:10.1046/j.1365-3113x.1998.00343.x
- 846 Collonnier C, Guyon-Debast A, Maclot F, Mara K, Charlot F, Nogué F (2017) Towards mastering
847 CRISPR-induced gene knock-in in plants: Survey of key features and focus on the model
848 *Physcomitrella patens*. *Methods* 121-122:103-117. doi:10.1016/j.ymeth.2017.04.024
- 849 Conn CE, Nelson DC (2016) Evidence that KARRIKIN-INSENSITIVE2 (KAI2) Receptors may
850 Perceive an Unknown Signal that is not Karrikin or Strigolactone. *Front Plant Sci* 6:1219.
851 doi:10.3389/fpls.2015.01219
- 852 Cook CE, Whichard LP, Turner B, Wall ME, Egley GH (1966) Germination of Witchweed (*Striga lutea*
853 Lour.): Isolation and Properties of a Potent Stimulant. *Science* 154 (3753):1189-1190
- 854 Coudert Y, Palubicki W, Ljung K, Novak O, Leyser O, Harrison CJ (2015) Three ancient hormonal cues
855 co-ordinate shoot branching in a moss. *Elife* 4. doi:10.7554/eLife.06808
- 856 de Saint Germain A, Clave G, Badet-Denisot MA, Pillot JP, Cornu D, Le Caer JP, Burger M, Pelissier
857 F, Retailleau P, Turnbull C, Bonhomme S, Chory J, Rameau C, Boyer FD (2016) An histidine
858 covalent receptor and butenolide complex mediates strigolactone perception. *Nat Chem Biol* 12
859 (10):787-794. doi:10.1038/nchembio.2147
- 860 de Saint Germain A, Jacobs A, Brun G, Pouvreau JB, Braem L, Cornu D, Clavé G, Baudu E, Steinmetz
861 V, Servajean V, Wicke S, Gevaert K, Simier P, Goormachtig S, Delavault P, Boyer FD (2021)
862 A *Phelipanche ramosa* KAI2 protein perceives strigolactones and isothiocyanates
863 enzymatically. *Plant Commun* 2 (5):100166. doi:10.1016/j.xplc.2021.100166
- 864 Decker EL, Alder A, Hunn S, Ferguson J, Lehtonen MT, Scheler B, Kerres KL, Wiedemann G, Safavi-
865 Rizi V, Nordzиеke S, Balakrishna A, Baz L, Avalos J, Valkonen JPT, Reski R (2017)
866 Strigolactone biosynthesis is evolutionarily conserved, regulated by phosphate starvation and
867 contributes to resistance against phytopathogenic fungi in a moss, *Physcomitrella patens*. *New*
868 *Phytol* 216 (2):455-468. doi:10.1111/nph.14506

- 869 Delaux PM, Xie X, Timme RE, Puech-Pages V, Dunand C, Lecompte E, Delwiche CF, Yoneyama K,
870 Becard G, Sejalon-Delmas N (2012) Origin of strigolactones in the green lineage. *New Phytol*
871 195 (4):857-871. doi:10.1111/j.1469-8137.2012.04209.x
- 872 Gomez-Roldan V, Fermas S, Brewer PB, Puech-Pages V, Dun EA, Pillot JP, Letisse F, Matusova R,
873 Danoun S, Portais JC, Bouwmeester H, Becard G, Beveridge CA, Rameau C, Rochange SF
874 (2008) Strigolactone inhibition of shoot branching. *Nature* 455 (7210):189-194.
875 doi:10.1038/nature07271
- 876 Guercio AM, Torabi S, Cornu D, Dalmais M, Bendahmane A, Le Signor C, Pillot JP, Le Bris P, Boyer
877 FD, Rameau C, Gutjahr C, de Saint Germain A, Shabek N (2022) Structural and functional
878 analyses explain Pea KAI2 receptor diversity and reveal stereoselective catalysis during signal
879 perception. *Commun Biol* 5 (1):126. doi:10.1038/s42003-022-03085-6
- 880 Hoffmann B, Proust H, Belcram K, Labrune C, Boyer FD, Rameau C, Bonhomme S (2014)
881 Strigolactones inhibit caulonema elongation and cell division in the moss *Physcomitrella patens*.
882 *PLoS One* 9 (6):e99206. doi:10.1371/journal.pone.0099206
- 883 Jiang L, Liu X, Xiong G, Liu H, Chen F, Wang L, Meng X, Liu G, Yu H, Yuan Y, Yi W, Zhao L, Ma
884 H, He Y, Wu Z, Melcher K, Qian Q, Xu HE, Wang Y, Li J (2013) DWARF 53 acts as a repressor
885 of strigolactone signalling in rice. *Nature* 504 (7480):401-405. doi:10.1038/nature12870
- 886 Jones D.T., Taylor W.R., and Thornton J.M. (1992) The rapid generation of mutation data matrices from
887 protein sequences. *Computer Applications in the Biosciences* 8: 275-282.
- 888 Karimi M, Bleys A, Vanderhaeghen R, Hilson P (2007) Building blocks for plant gene assembly. *Plant*
889 *Physiol* 145 (4):1183-1191. doi:10.1104/pp.107.110411
- 890 Kerr SC, Patil SB, de Saint Germain A, Pillot JP, Saffar J, Ligerot Y, Aubert G, Citerne S, Bellec Y,
891 Dun EA, Beveridge CA, Rameau C (2021) Integration of the SMXL/D53 strigolactone
892 signalling repressors in the model of shoot branching regulation in *Pisum sativum*. *Plant J* 107
893 (6):1756-1770. doi:10.1111/tpj.15415
- 894 Khosla A, Morffy N, Li Q, Faure L, Chang SH, Yao J, Zheng J, Cai ML, Stanga J, Flematti GR, Waters
895 MT, Nelson DC (2020) Structure-Function Analysis of SMAX1 Reveals Domains That Mediate
896 Its Karrikin-Induced Proteolysis and Interaction with the Receptor KAI2. *Plant Cell* 32
897 (8):2639-2659. doi:10.1105/tpc.19.00752
- 898 Kodama K, Rich MK, Yoda A, Shimazaki S, Xie X, Akiyama K, Mizuno Y, Komatsu A, Luo Y, Suzuki
899 H, Kameoka H, Libourel C, Keller J, Sakakibara K, Nishiyama T, Nakagawa T, Mashiguchi K,
900 Uchida K, Yoneyama K, Tanaka Y, Yamaguchi S, Shimamura M, Delaux PM, Nomura T,
901 Kyojuka J (2022) An ancestral function of strigolactones as symbiotic rhizosphere signals. *Nat*
902 *Commun* 13 (1):3974. doi:10.1038/s41467-022-31708-3
- 903 Kumar S., Stecher G., Li M., Knyaz C., and Tamura K. (2018) MEGA X: Molecular Evolutionary
904 Genetics Analysis across computing platforms. *Molecular Biology and Evolution* 35:1547-
905 1549.
- 906 Kyojuka J, Nomura T, Shimamura M (2022) Origins and evolution of the dual functions of
907 strigolactones as rhizosphere signaling molecules and plant hormones. *Curr Opin Plant Biol*
908 65:102154. doi:10.1016/j.pbi.2021.102154
- 909 Le Bail A, Scholz S, Kost B (2013) Evaluation of reference genes for RT qPCR analyses of structure-
910 specific and hormone regulated gene expression in *Physcomitrella patens* gametophytes. *PLoS*
911 *One* 8 (8):e70998. doi:10.1371/journal.pone.0070998
- 912 Liang Y, Ward S, Li P, Bennett T, Leyser O (2016) SMAX1-LIKE7 Signals from the Nucleus to
913 Regulate Shoot Development in *Arabidopsis* via Partially EAR Motif-Independent
914 Mechanisms. *Plant Cell* 28 (7):1581-1601. doi:10.1105/tpc.16.00286
- 915 Lopez-Obando M, Conn CE, Hoffmann B, Bythell-Douglas R, Nelson DC, Rameau C, Bonhomme S
916 (2016a) Structural modelling and transcriptional responses highlight a clade of PpKAI2-LIKE
917 genes as candidate receptors for strigolactones in *Physcomitrella patens*. *Planta* 243 (6):1441-
918 1453. doi:10.1007/s00425-016-2481-y
- 919 Lopez-Obando M, de Villiers R, Hoffmann B, Ma L, de Saint Germain A, Kossmann J, Coudert Y,
920 Harrison CJ, Rameau C, Hills P, Bonhomme S (2018) *Physcomitrella patens* MAX2
921 characterization suggests an ancient role for this F-box protein in photomorphogenesis rather
922 than strigolactone signalling. *New Phytol* 219 (2):743-756. doi:10.1111/nph.15214

- 923 Lopez-Obando M, Guillory A, Boyer FD, Cornu D, Hoffmann B, Le Bris P, Pouvreau JB, Delavault P,
924 Rameau C, de Saint Germain A, Bonhomme S (2021) The Physcomitrium (*Physcomitrella*)
925 patens PpKAI2L receptors for strigolactones and related compounds function via MAX2-
926 dependent and -independent pathways. *Plant Cell* 33 (11):3487-3512.
927 doi:10.1093/plcell/koab217
- 928 Lopez-Obando M, Hoffmann B, Géry C, Guyon-Debast A, Téoulé E, Rameau C, Bonhomme S, Nogué
929 F (2016b) Simple and Efficient Targeting of Multiple Genes Through CRISPR-Cas9 in
930 *Physcomitrella patens*. *G3 (Bethesda)* 6 (11):3647-3653. doi:10.1534/g3.116.033266
- 931 Ma H, Duan J, Ke J, He Y, Gu X, Xu TH, Yu H, Wang Y, Brunzelle JS, Jiang Y, Rothbart SB, Xu HE,
932 Li J, Melcher K (2017) A D53 repression motif induces oligomerization of TOPLESS
933 corepressors and promotes assembly of a corepressor-nucleosome complex. *Science advances*
934 3 (6):e1601217. doi:10.1126/sciadv.1601217
- 935 Machin DC, Hamon-Josse M, Bennett T (2020) Fellowship of the rings: a saga of strigolactones and
936 other small signals. *New Phytol* 225 (2):621-636. doi:10.1111/nph.16135
- 937 Mizuno Y, Komatsu A, Shimazaki S, Naramoto S, Inoue K, Xie X, Ishizaki K, Kohchi T, Kyojuka J
938 (2021) Major components of the KARRIKIN INSENSITIVE2-dependent signaling pathway are
939 conserved in the liverwort *Marchantia polymorpha*. *Plant Cell* 33 (7):2395-2411.
940 doi:10.1093/plcell/koab106
- 941 Moturu TR, Thula S, Singh RK, Nodzynski T, Vareková RS, Friml J, Simon S (2018) Molecular
942 evolution and diversification of the SMXL gene family. *J Exp Bot* 69 (9):2367-2378.
943 doi:10.1093/jxb/ery097
- 944 Ortiz-Ramirez C, Hernandez-Coronado M, Thamm A, Catarino B, Wang M, Dolan L, Feijo JA, Becker
945 JD (2016) A Transcriptome Atlas of *Physcomitrella patens* Provides Insights into the Evolution
946 and Development of Land Plants. *Mol Plant* 9 (2):205-220. doi:10.1016/j.molp.2015.12.002
- 947 Perroud PF, Haas FB, Hiss M, Ullrich KK, Alboresi A, Amirebrahimi M, Barry K, Bassi R, Bonhomme
948 S, Chen H, Coates JC, Fujita T, Guyon-Debast A, Lang D, Lin J, Lipzen A, Nogué F, Oliver
949 MJ, Ponce de León I, Quatrano RS, Rameau C, Reiss B, Reski R, Ricca M, Saidi Y, Sun N,
950 Szövényi P, Sreedasyam A, Grimwood J, Stacey G, Schmutz J, Rensing SA (2018) The
951 *Physcomitrella patens* gene atlas project: large-scale RNA-seq based expression data. *Plant J* 95
952 (1):168-182. doi:10.1111/tpj.13940
- 953 Proust H, Hoffmann B, Xie X, Yoneyama K, Schaefer DG, Nogue F, Rameau C (2011) Strigolactones
954 regulate protonema branching and act as a quorum sensing-like signal in the moss
955 *Physcomitrella patens*. *Development* 138 (8):1531-1539. doi:10.1242/dev.058495
- 956 Radhakrishnan GV, Keller J, Rich MK, Vernié T, Mbadinga Mbadinga DL, Vigneron N, Cottret L,
957 Clemente HS, Libourel C, Cheema J, Linde AM, Eklund DM, Cheng S, Wong GKS,
958 Lagercrantz U, Li FW, Oldroyd GED, Delaux PM (2020) An ancestral signalling pathway is
959 conserved in intracellular symbioses-forming plant lineages. *Nat Plants* 6 (3):280-289.
960 doi:10.1038/s41477-020-0613-7
- 961 Soundappan I, Bennett T, Morffy N, Liang Y, Stanga JP, Abbas A, Leyser O, Nelson D (2015) SMAX1-
962 LIKE/D53 Family Members Enable Distinct MAX2-Dependent Responses to Strigolactones
963 and Karrikins in *Arabidopsis*. *Plant Cell* 27 (11):3143-3159. doi:10.1105/tpc.15.00562
- 964 Stanga JP, Morffy N, Nelson DC (2016) Functional redundancy in the control of seedling growth by the
965 karrikin signaling pathway. *Planta* 243 (6):1397-1406. doi:10.1007/s00425-015-2458-2
- 966 Stanga JP, Smith SM, Briggs WR, Nelson DC (2013) SUPPRESSOR OF MORE AXILLARY
967 GROWTH2 1 controls seed germination and seedling development in *Arabidopsis*. *Plant*
968 *Physiol* 163 (1):318-330. doi:10.1104/pp.113.221259
- 969 Sun YK, Flematti GR, Smith SM, Waters MT (2016) Reporter Gene-Facilitated Detection of
970 Compounds in *Arabidopsis* Leaf Extracts that Activate the Karrikin Signaling Pathway. *Front*
971 *Plant Sci* 7:1799. doi:10.3389/fpls.2016.01799
- 972 Temmerman A, Guillory A, Bonhomme S, Goormachtig S, Struk S (2022) Masks Start to Drop:
973 Suppressor of MAX2 1-Like Proteins Reveal Their Many Faces. *Front Plant Sci* 13:887232.
974 doi:10.3389/fpls.2022.887232
- 975 Umehara M, Hanada A, Yoshida S, Akiyama K, Arite T, Takeda-Kamiya N, Magome H, Kamiya Y,
976 Shirasu K, Yoneyama K, Kyojuka J, Yamaguchi S (2008) Inhibition of shoot branching by new
977 terpenoid plant hormones. *Nature* 455 (7210):195-200. doi:10.1038/nature07272

- 978 Walker CH, Siu-Ting K, Taylor A, O'Connell MJ, Bennett T (2019) Strigolactone synthesis is ancestral
979 in land plants, but canonical strigolactone signalling is a flowering plant innovation. *BMC*
980 *biology* 17 (1):70. doi:10.1186/s12915-019-0689-6
- 981 Wallner ES, López-Salmerón V, Belevich I, Poschet G, Jung I, Grünwald K, Sevillem I, Jokitalo E, Hell
982 R, Helariutta Y, Agustí J, Lebovka I, Greb T (2017) Strigolactone- and Karrikin-Independent
983 SMXL Proteins Are Central Regulators of Phloem Formation. *Curr Biol* 27 (8):1241-1247.
984 doi:10.1016/j.cub.2017.03.014
- 985 Wallner ES, Tonn N, Shi D, Jouannet V, Greb T (2020) SUPPRESSOR OF MAX2 1-LIKE 5 promotes
986 secondary phloem formation during radial stem growth. *Plant J* 102 (5):903-915.
987 doi:10.1111/tpj.14670
- 988 Wang L, Wang B, Jiang L, Liu X, Li X, Lu Z, Meng X, Wang Y, Smith SM, Li J (2015) Strigolactone
989 Signaling in Arabidopsis Regulates Shoot Development by Targeting D53-Like SMXL
990 Repressor Proteins for Ubiquitination and Degradation. *Plant Cell* 27 (11):3128-3142.
991 doi:10.1105/tpc.15.00605
- 992 Wang L, Wang B, Yu H, Guo H, Lin T, Kou L, Wang A, Shao N, Ma H, Xiong G, Li X, Yang J, Chu
993 J, Li J (2020) Transcriptional regulation of strigolactone signalling in Arabidopsis. *Nature* 583
994 (7815):277-281. doi:10.1038/s41586-020-2382-x
- 995 Waters MT, Scaffidi A, Moulin SL, Sun YK, Flematti GR, Smith SM (2015) A *Selaginella*
996 *moellendorffii* Ortholog of KARRIKIN INSENSITIVE2 Functions in Arabidopsis
997 Development but Cannot Mediate Responses to Karrikins or Strigolactones. *Plant Cell* 27
998 (7):1925-1944. doi:10.1105/tpc.15.00146
- 999 Yao J, Scaffidi A, Meng Y, Melville KT, Komatsu A, Khosla A, Nelson DC, Kyoizuka J, Flematti GR,
1000 Waters MT (2021) Desmethyl butenolides are optimal ligands for karrikin receptor proteins.
1001 *New Phytol* 230 (3):1003-1016. doi:10.1111/nph.17224
- 1002 Zheng J, Hong K, Zeng L, Wang L, Kang S, Qu M, Dai J, Zou L, Zhu L, Tang Z, Meng X, Wang B, Hu
1003 J, Zeng D, Zhao Y, Cui P, Wang Q, Qian Q, Wang Y, Li J, Xiong G (2020) Karrikin Signaling
1004 Acts Parallel to and Additively with Strigolactone Signaling to Regulate Rice Mesocotyl
1005 Elongation in Darkness. *Plant Cell* 32 (9):2780-2805. doi:10.1105/tpc.20.00123
- 1006 Zhou F, Lin Q, Zhu L, Ren Y, Zhou K, Shabek N, Wu F, Mao H, Dong W, Gan L, Ma W, Gao H, Chen
1007 J, Yang C, Wang D, Tan J, Zhang X, Guo X, Wang J, Jiang L, Liu X, Chen W, Chu J, Yan C,
1008 Ueno K, Ito S, Asami T, Cheng Z, Lei C, Zhai H, Wu C, Wang H, Zheng N, Wan J (2013) D14-
1009 SCF(D3)-dependent degradation of D53 regulates strigolactone signalling. *Nature* 504
1010 (7480):406-410. doi:10.1038/nature12878
- 1011

Figure 1

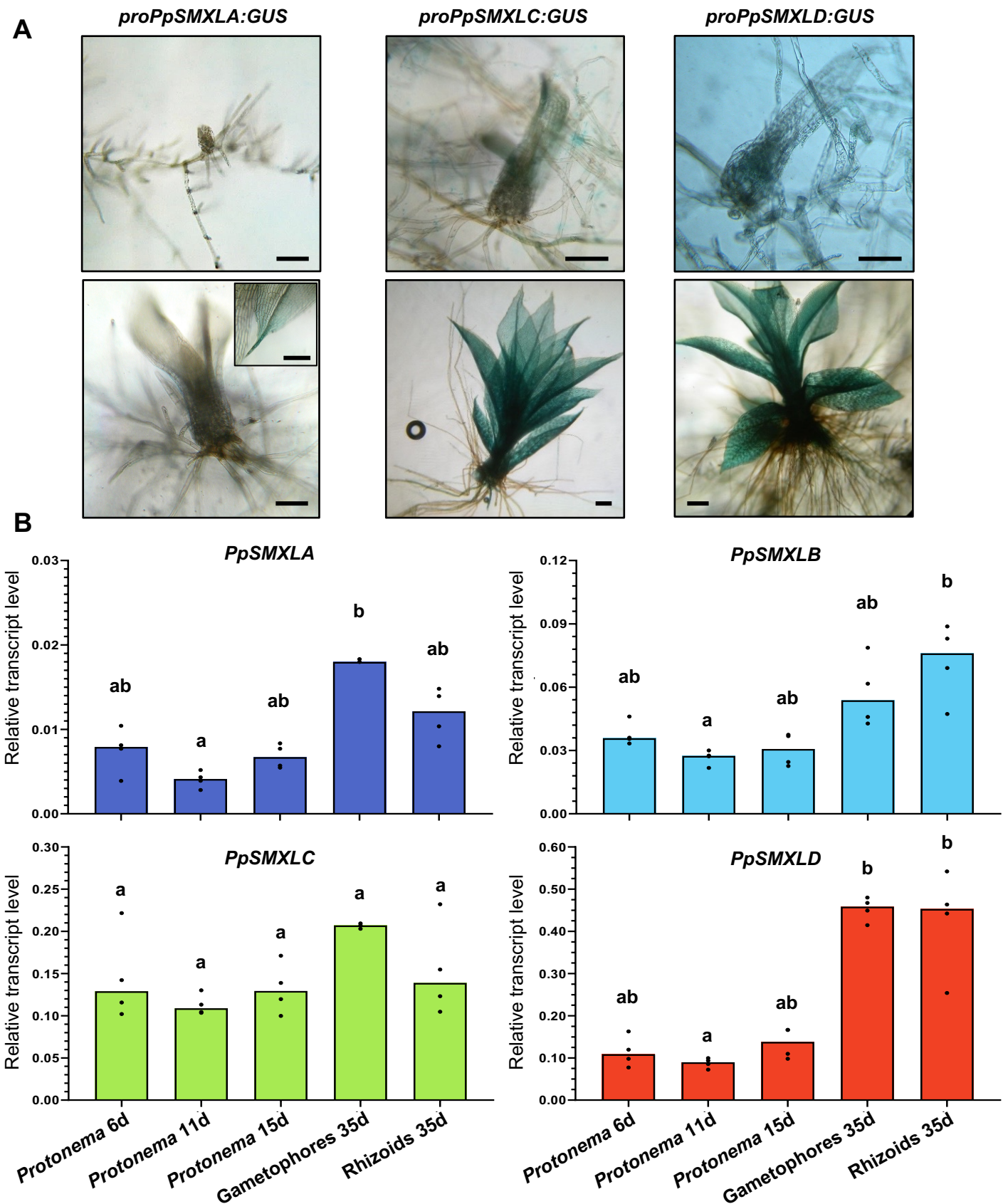
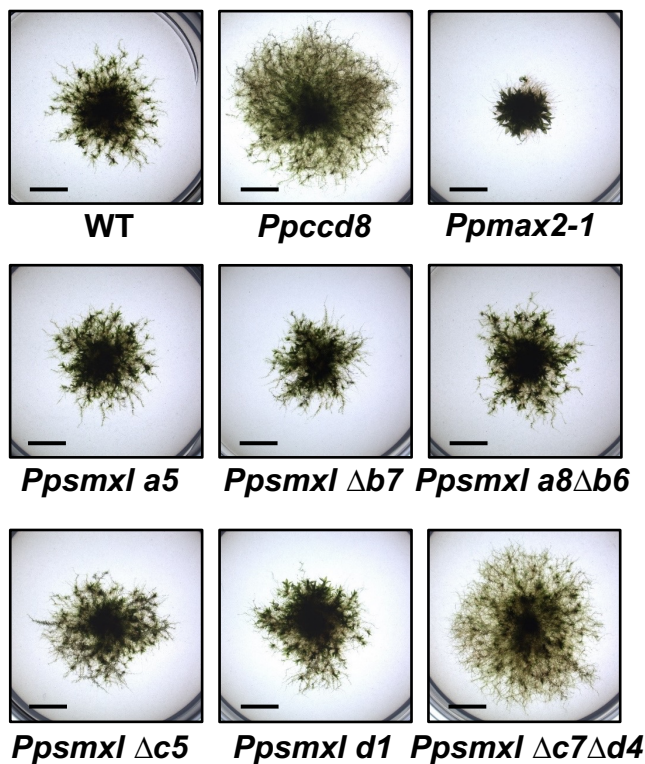


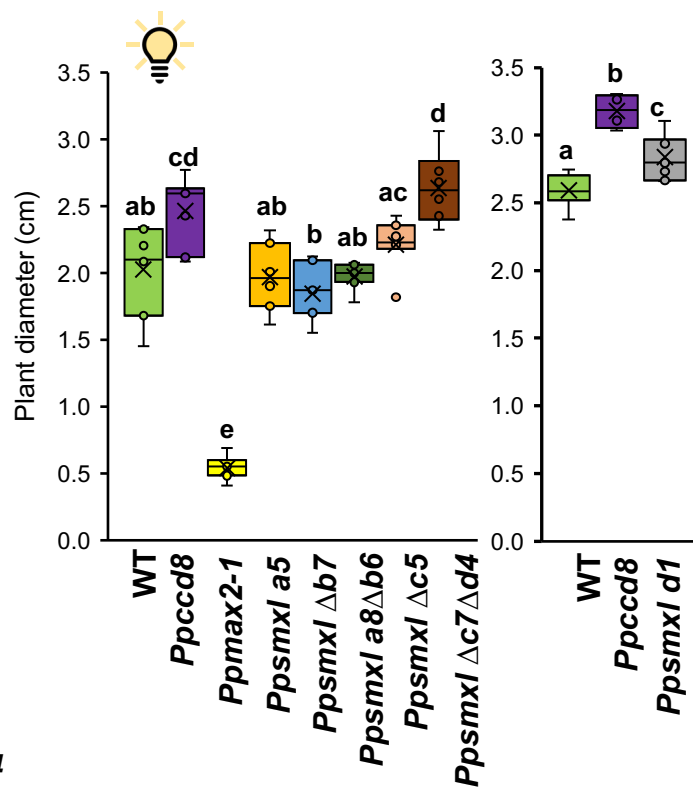
Figure 1 Expression of *PpSMXL* genes along *P. patens* vegetative development. A, GUS staining of 2-week old *proPpSMXL:GUS* plants. Scale bars = 500 μ m. B, Transcript levels of the four *PpSMXL* genes, relative to the two reference genes *PpACT3* (*Pp3c10_17080*) and *PpAPT* (*Pp3c8_16590*). RT-qPCR data used for the analysis was extracted from 4 biological replicates, each with 2 technical repeats. Each point represents the mean of two technical repeats. Some points were excluded from analysis following an outliers identification test carried out in GraphPad Prism (version 8.4.2). Statistical significance scores of comparisons among tissues are indicated as bold letters (Kruskal-Wallis test followed by a Dunn *post-hoc* test, $p < 5\%$). Note the difference in expression values on y axes.

Figure 2

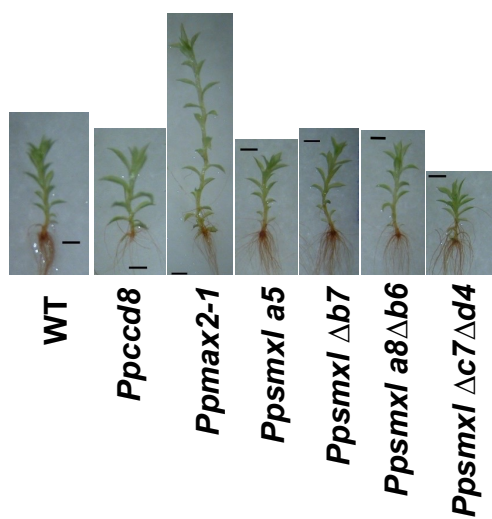
A



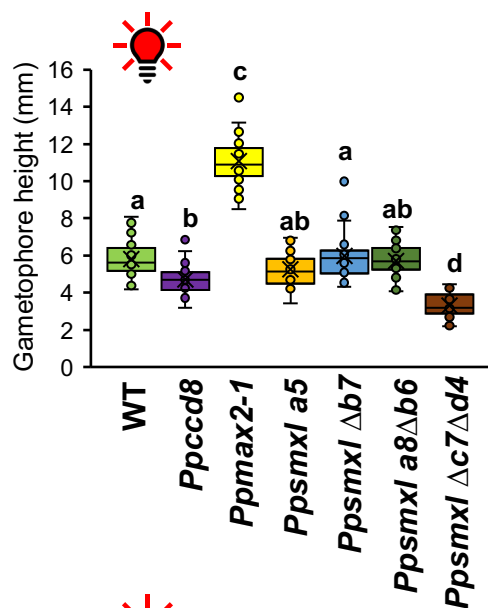
B



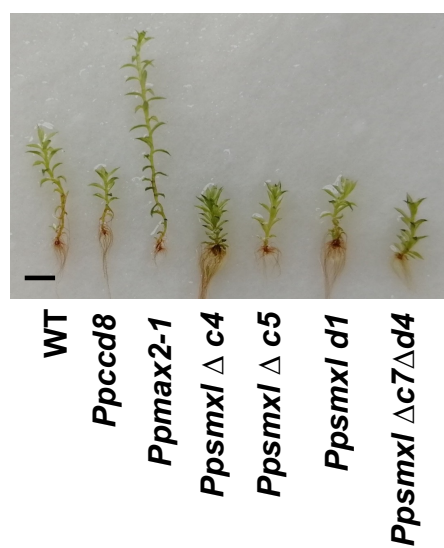
C



D



E



F

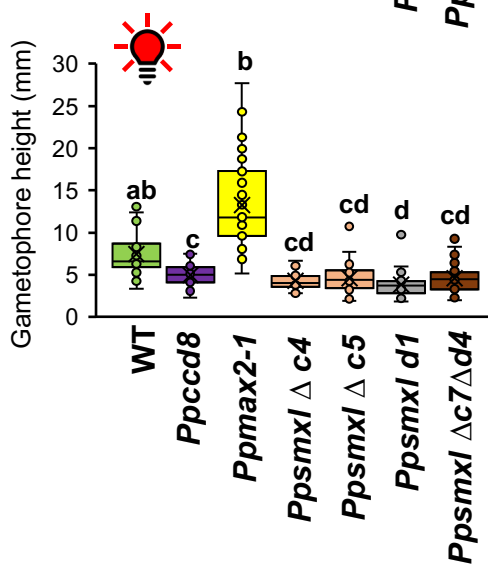


Figure 2 Phenotypes of the *Ppsmx1* mutants. *Ppsmx1* mutants were grown in white light long day conditions (A-B) , or under continuous red light (C-F).

A, Three-week-old plants grown in the light on low nitrogen content medium, without underlying cellophane. Bar = 5 mm. B, Diameters of six-week-old plants; n=35-49 plants of each genotype grown on 7 individual plates. Statistical significance of comparisons between all genotypes are indicated by bold symbols; left panel: Kruskal Wallis followed by a Dunn *post-hoc* test, n=42-49, p<5%; right panel: standard ANOVA followed by a Tukey *post-hoc* test, n=20-35, p<5%). C, E, Examples of gametophores from two-month-old plants grown in red light. Bar = 3 mm D, F, Gametophore height measured for 30 two-month-old gametophores of each genotype. Statistical significance of comparisons between all genotypes are indicated by bold symbols, Kruskal Wallis followed by a Dunn *post-hoc* test, n≥30, p<5%.

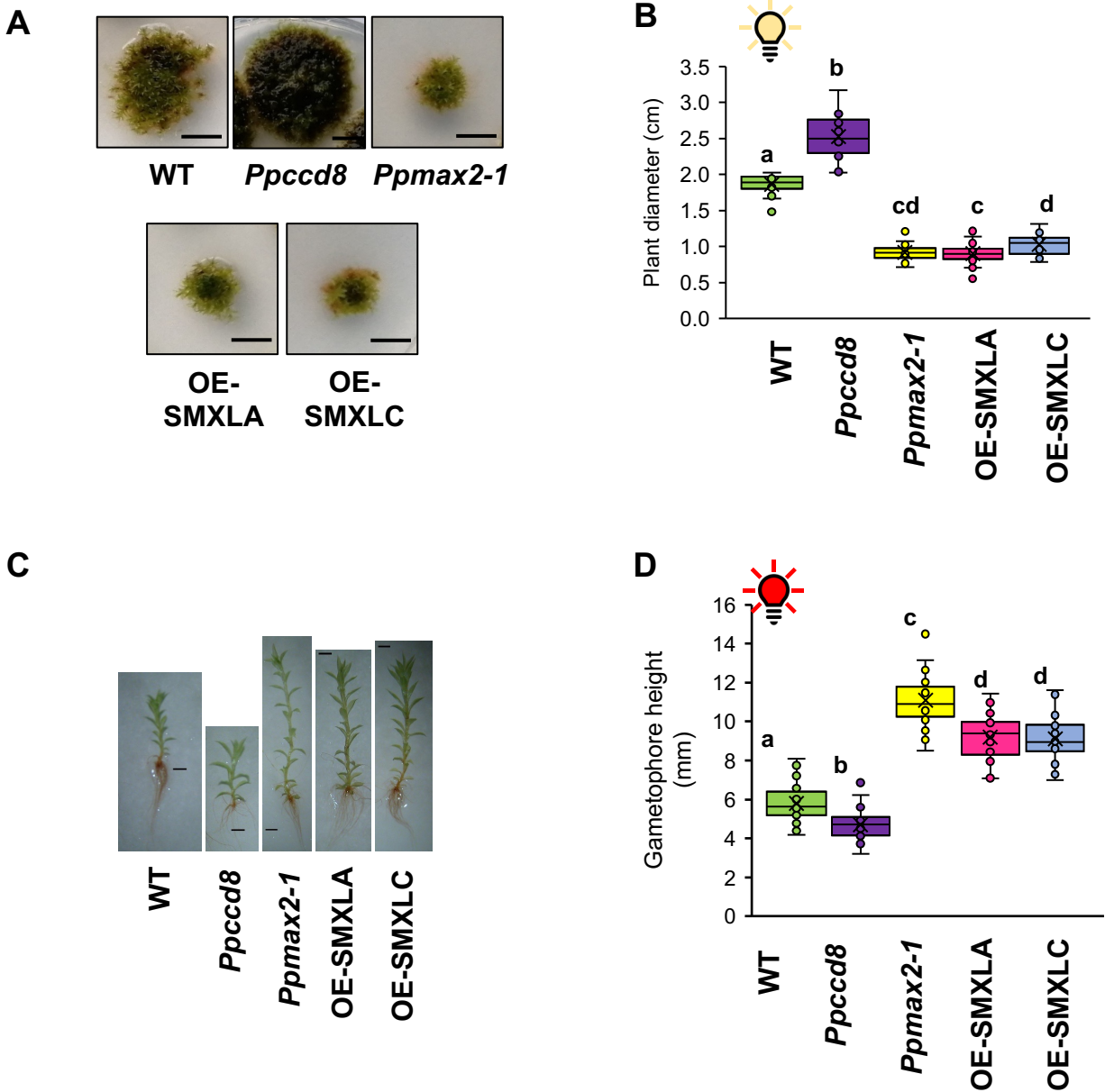


Figure 3 Growth of *proZmUbi:GFP-PpSMXL* lines. (A-B): Plant extension in control conditions. A, Representative individuals after 5 weeks of growth. Scale bar = 1 cm. B, Diameters were measured from 6 week-old plants, $n = 21-35$, grown on at least 3 different plates. Statistical significance of comparisons between all genotypes are indicated as bold symbols (Welch ANOVA followed by a Dunnett post-hoc test, $p < 5\%$). (C-D) Gametophore height in red light. C, Representative individuals after two months culture under continuous red light. Scale bar = 1 mm. D, Gametophore height was measured for $n = 28-30$ two-month-old gametophores of each genotype. Statistical significance of comparisons between all genotypes are indicated by bold symbols (standard ANOVA followed by a Tukey *post-hoc* test, $p < 5\%$).

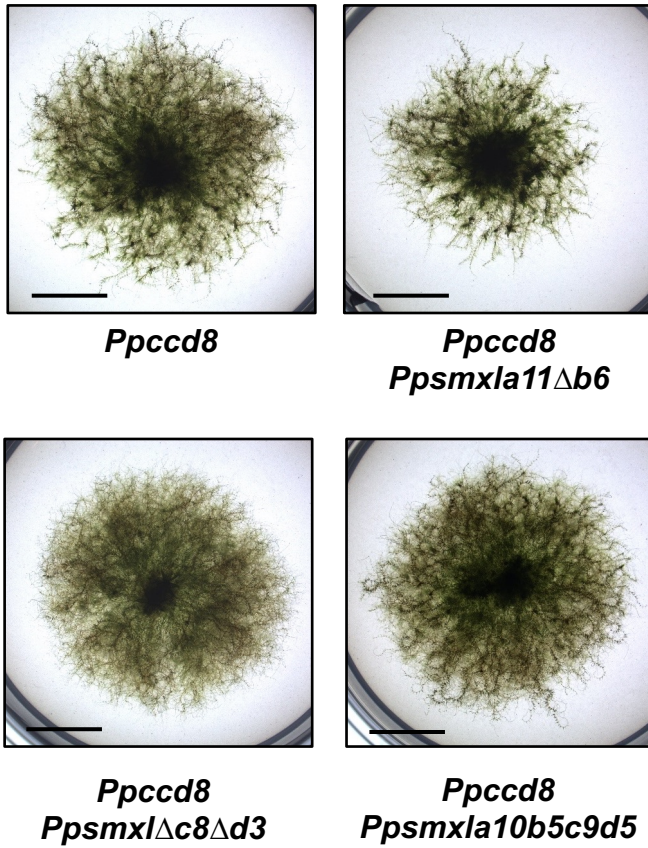
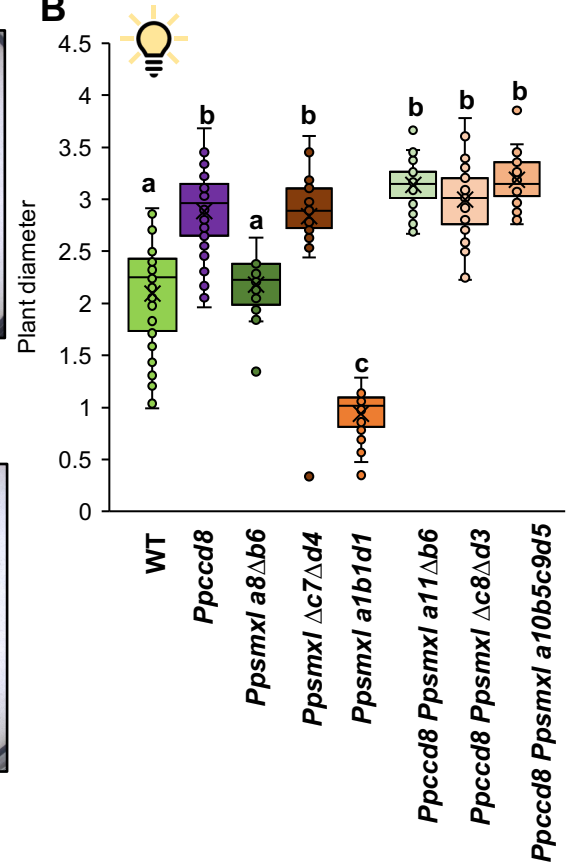
A**B**

Figure 4 Genetic analysis of *PpSMXL* relationship with *PpCCD8*. A, Phenotype of three-week-old plants on low nitrogen content medium (without underlying cellophane). Scale bar = 5 mm. B, Extension phenotype of some of these mutants on low nitrogen content medium (with underlying cellophane), after 5 weeks growth. Statistical significance of comparisons relative to WT at the last time point is shown as bold black letters (Kruskal Wallis followed by a Dunn *post-hoc* test, $n = 35-40$, $p < 5\%$).

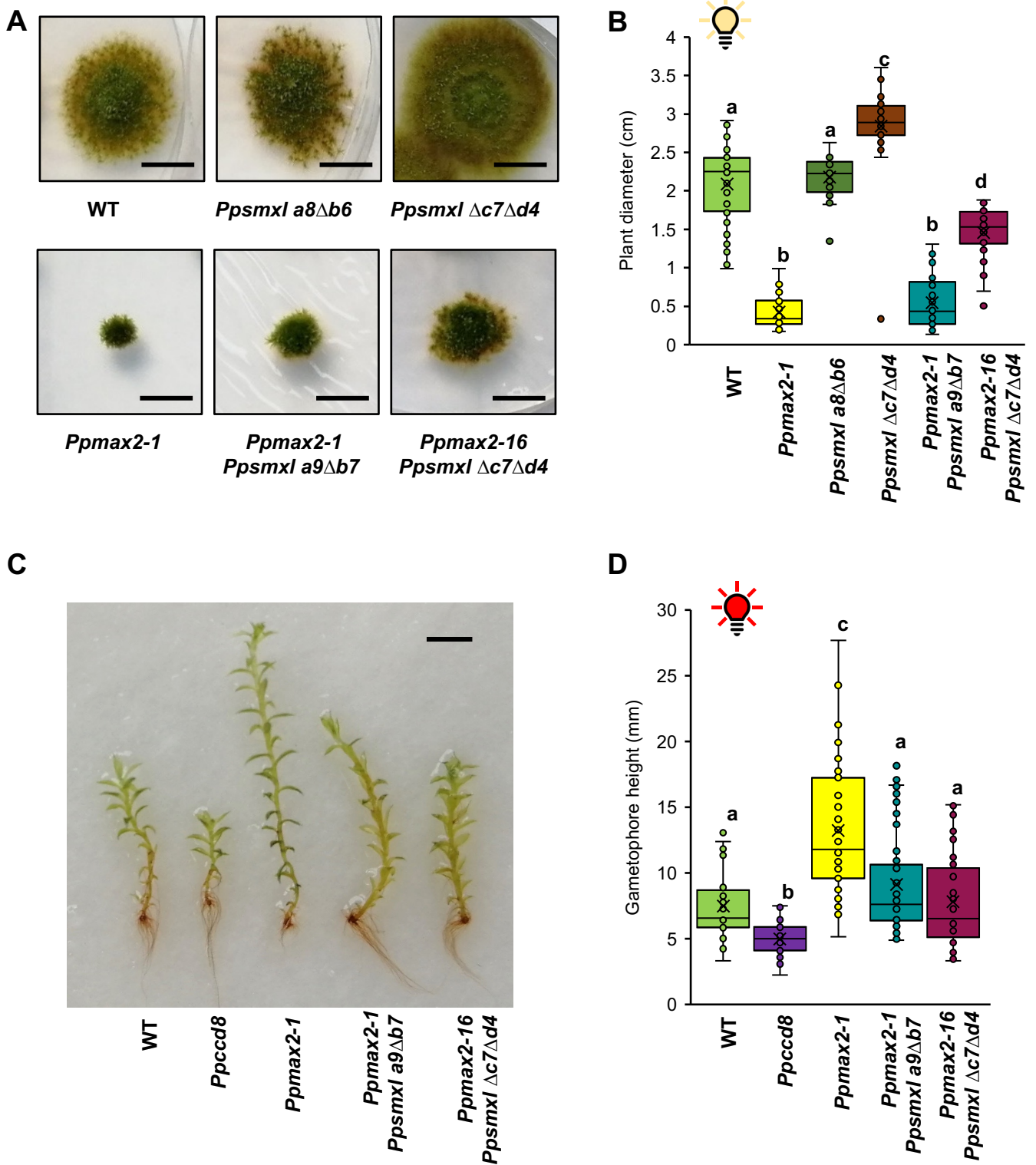


Figure 5 Genetic analysis of *PpSMXL* relationship with *PpMAX2*. (A-B): Plant extension in control conditions. A, Representative individuals after 5 weeks of growth. Bar = 1 cm. B, Plant diameters of the mutants grown on low nitrogen content medium with underlying cellophane for 5 weeks. $N \geq 35$ individuals grown on 7 different plates. (C-D) Gametophore height in red light. C, Representative gametophores after two months culture under constant red light. Scale bar = 3 mm. D, Gametophore height was measured for 30 two-month-old gametophores of each genotype. Each point represents a measurement. $N \geq 43$ gametophores from 3 different Magenta boxes. (B,D): Statistical significance of comparisons between all genotypes are indicated by bold letters (Kruskal Wallis followed by a Dunn *post-hoc* test, $p < 0.05$).

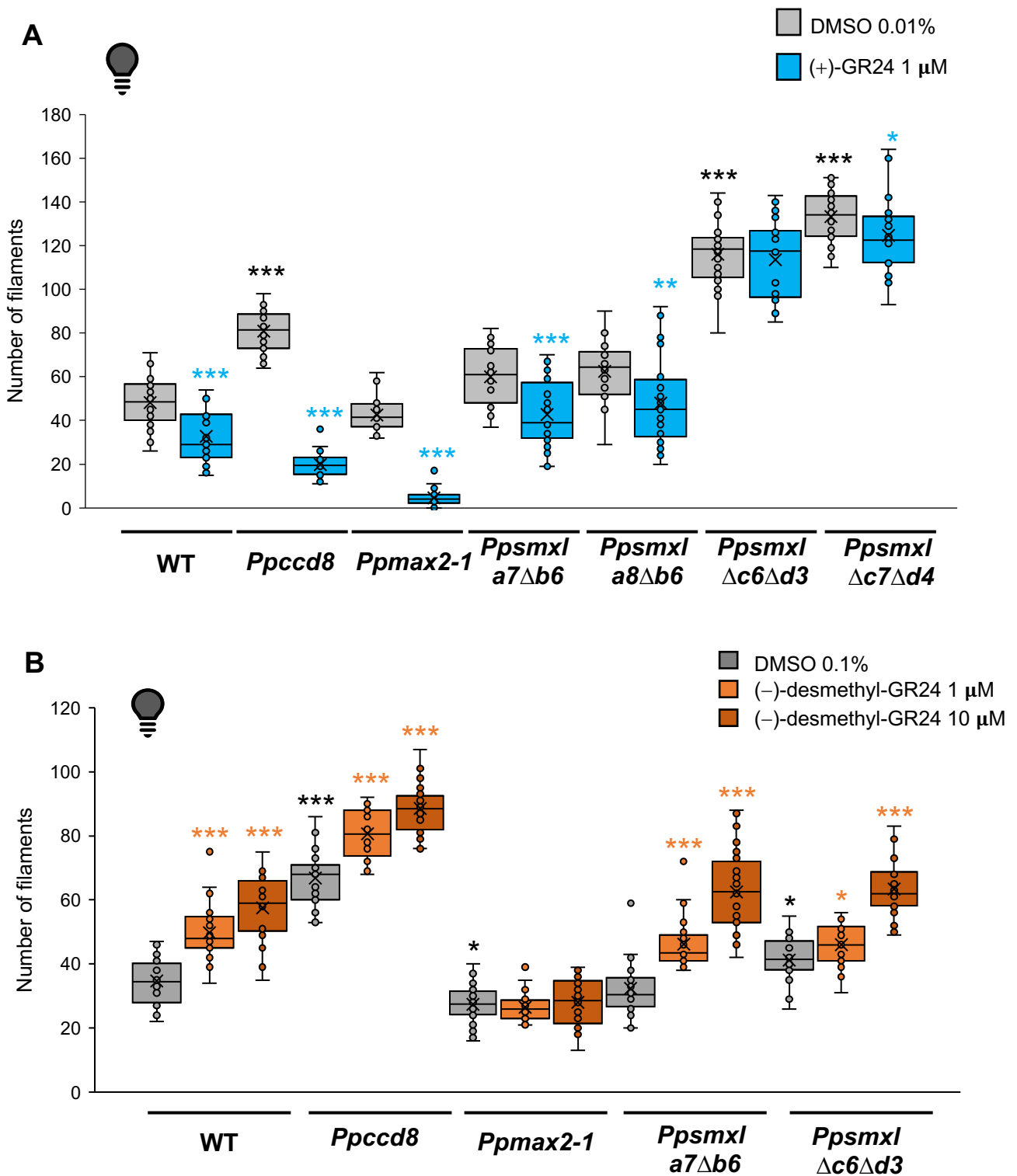


Figure 6 *Ppsmx1* mutant response to (\pm)-GR24 enantiomers. A, Response to (+)-GR24: $n = 24$ two-week-old plants of each genotype were mock treated with 0,01% DMSO (grey) or with 1 μ M of (+)-GR24 (blue). Plants were incubated vertically in the dark for ten days. Negatively gravitropic caulonema filaments were enumerated for each plant. Statistical significance of comparisons of control groups relative to WT is shown as black symbols (Kruskal Wallis followed by a Dunn *post-hoc* test). Statistical significance of comparisons between control and treated for each genotype is shown as blue symbols (Mann-Whitney tests).

B, Response to (-)-desmethyl-GR24: $n = 24$ two-week-old plants of each genotype were mock treated with 0,01% DMSO (grey), 1 μ M of (-)-desmethyl-GR24 (orange) or 10 μ M of (-)-desmethyl-GR24 (brown). Statistical significance of comparisons of control groups relative to WT is shown as black symbols (Kruskal Wallis followed by a Dunn *post-hoc* test). Statistical significance of comparisons between control and treated for each genotype is shown as orange symbols (Kruskal Wallis tests followed by Tukey *post-hoc* tests).

A and B. For all statistical analyses, p -values are reported as * $0.01 \leq p < 0.05$, ** $0.001 \leq p < 0.01$, *** $p < 0.001$.

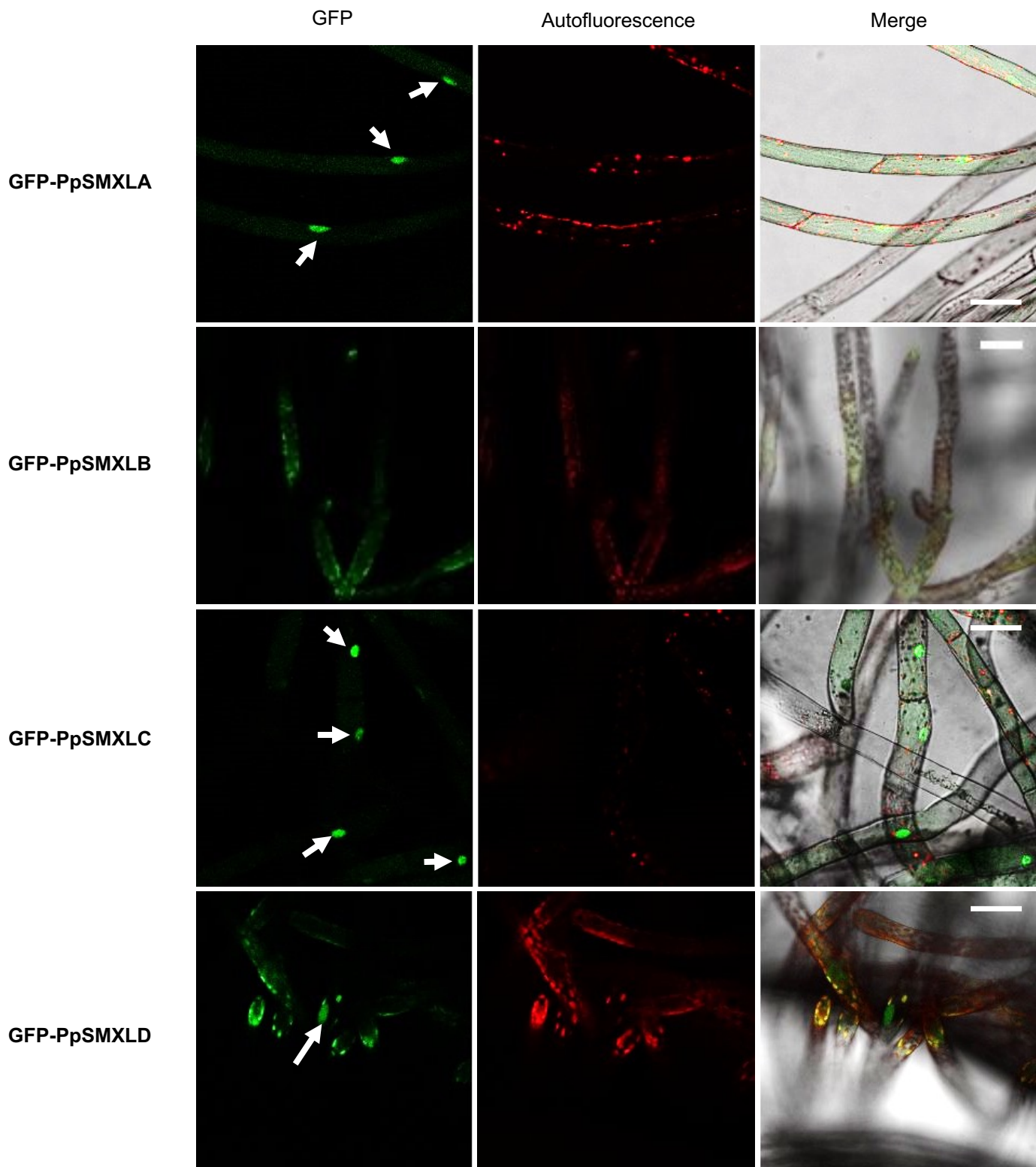


Figure 7 Subcellular localization of GFP-PpSMXL fusion proteins in *P. patens*. Confocal images of protonema filaments of transgenic *P. patens* lines expressing *proZmUbi::GFP-PpSMXL* fusions as indicated on the left. Right images are overlays of autofluorescence (red) and GFP (green) channels. Bar = 50 μ m. Arrow points to a nucleus.

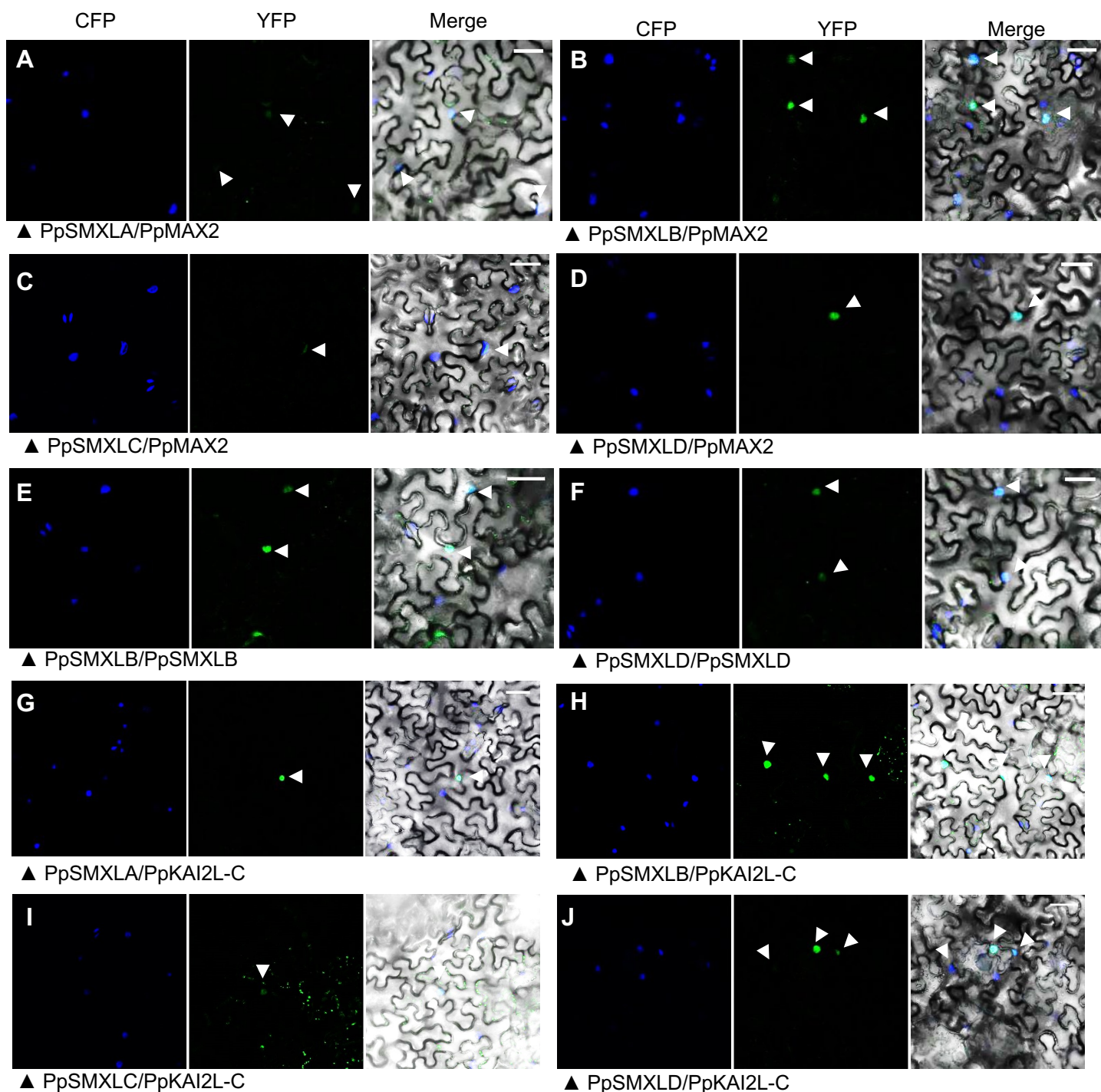


Figure 8 PpSMXL protein interaction assays in *Nicotiana benthamiana*. All four PpSMXL can interact with PpMAX2 (A-D). PpSMXLB and PpSMXLD can form homo-oligomers (E,F). All four PpSMXL can interact with PpKAI2L-C (G-J). Below each tryptic of images, the first indicated protein is fused to the N-terminal part of eYFP, while the second protein is fused to the C-terminal part (both tags are fused at the N-terminal end of *P. patens* proteins). Colocalization of CFP-H2b and eYFP biFC signals are pointed at with white arrows on. Merge are overlays of CFP (blue), YFP (green) and bright field images. Bar = 50 μ m. Tested interactions with DEFICIENS and GLOBOSA proteins from *Antirrhinum major* (negative controls) are shown in Supplemental Figure S17. The previously published GLOBOSA/DEFICIENS interaction (Azimzadeh et al., 2008) was consistently used a positive control of eYFP reconstruction.

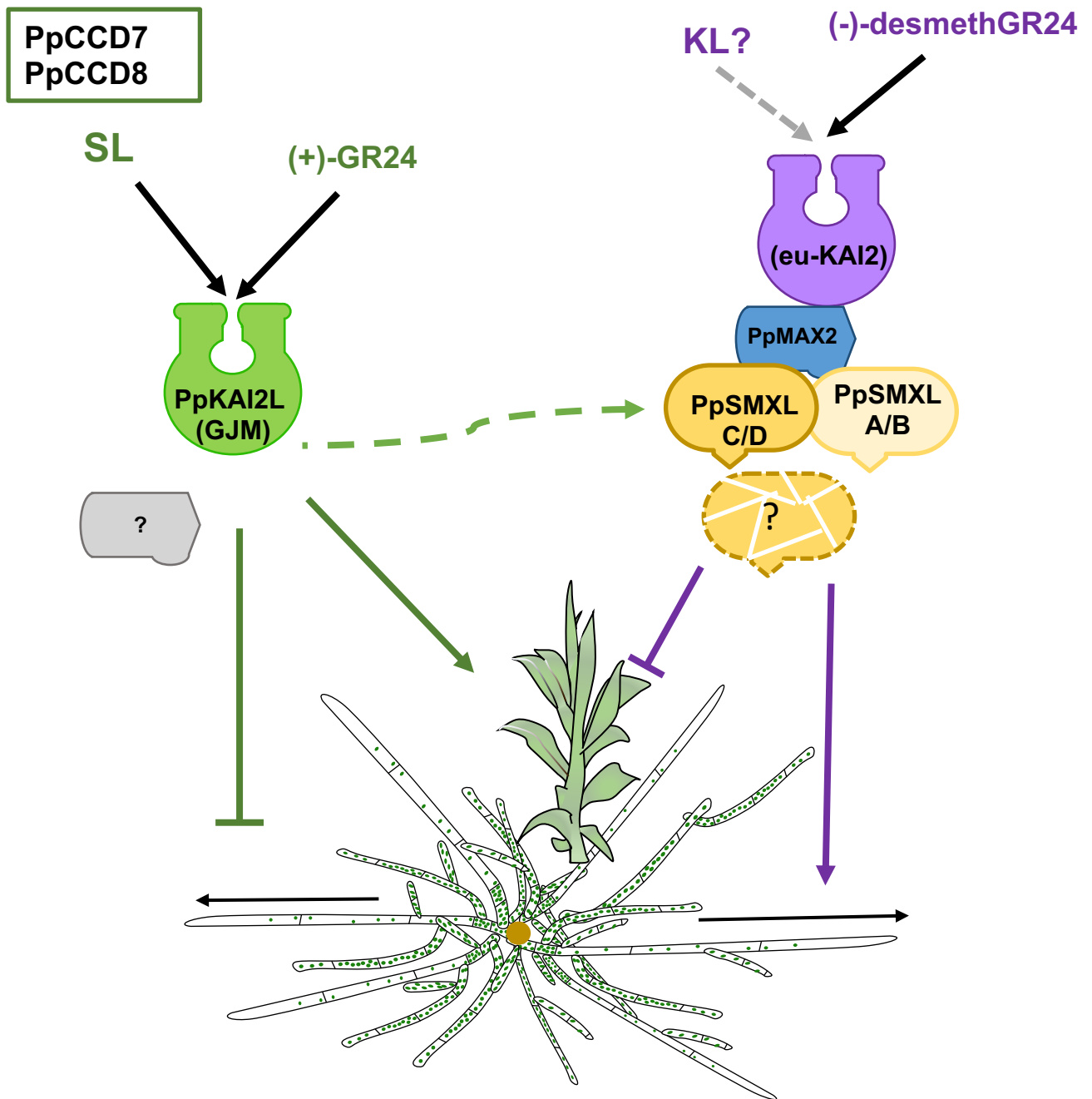


Figure 9 Current model of KL and SL signaling in *P. patens*. SLs and putative KL signal are mimicked by (+)-GR24 and (-)-desmethyl-GR24 respectively. The two pathways have opposite effects on protonema extension and gametophore development. In contrast to angiosperms, only the KL pathway is PpMAX2 dependent. All four PpSMXL are likely suppressors of the KL pathway, though their PpMAX2-dependent degradation following KL/(-)-desmethyl-GR24 perception has not been demonstrated (question mark). Green dotted arrow indicates that PpSMXL could be stabilized by SLs. A further level of regulation through possible transcriptional regulation of *PpSMXL* gene transcription by PpSMXL proteins has not been represented.

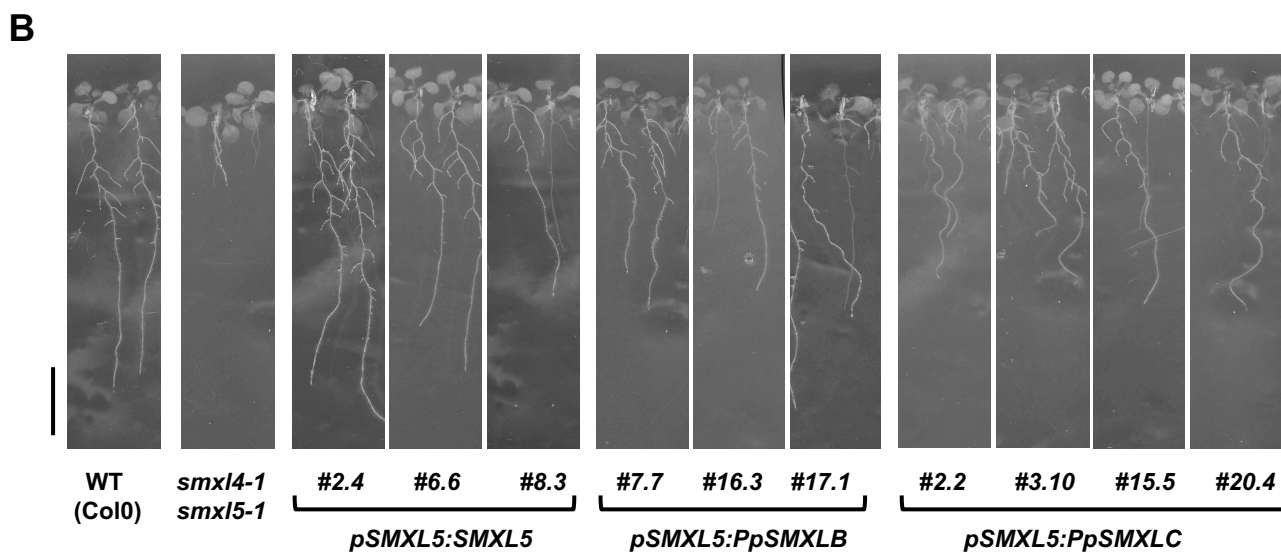
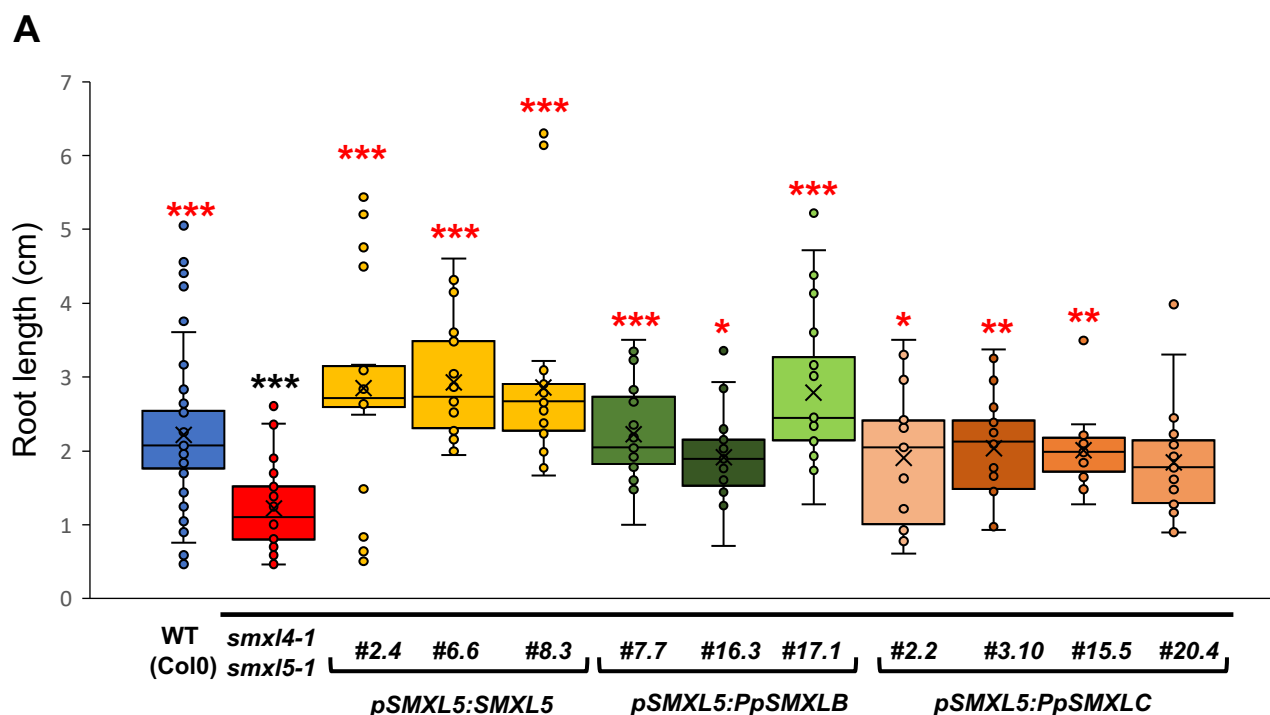


Figure 10 *Atsmxl4/5* mutant root phenotype is complemented by PpSMXLB and PpSMXLC. A, Root length was measured from 15 day-old seedlings grown vertically on 0.5 x MS with 1% sucrose. 20 to 40 seedlings per genotype, grown on 3 different plates. Statistical significance of comparisons relative to WT is shown as black symbols and statistical significance of comparisons relative to the double mutant *smxl4,5* is shown as red symbols (Kruskal Wallis followed by a Dunn *post-hoc* test, $p < 5\%$). B, Representative seedlings from each genotype. Scale bar = 1 cm